INFLUENCE OF COMPOSITION AND THERMOMECHANICAL PROCESSING CONDITIONS ON THE MICROSTRUCTURE AND PROPERTIES OF HOT ROLLED MICROALLOYED STEELS

by

Junyu Duan

B.S. in Materials Science and Engineering, Wuhan University of Technology, 2014

Submitted to the Graduate Faculty of

Swanson School of Engineering in partial fulfillment

of the requirements for the degree of

Master of Science

University of Pittsburgh

2016

UNIVERSITY OF PITTSBURGH

SWANSON SCHOOL OF ENGINEERING

This thesis was presented

by

Junyu Duan

It was defended on

March 25, 2016

and approved by

Scott Mao, Ph.D., Professor, Department of Mechanical Engineering and Materials Science

Patrick Smolinski, Ph.D., Associate Professor, Department of Mechanical Engineering and Materials Science

Thesis Advisor: Anthony J. DeArdo, Ph.D., Professor, Department of Mechanical Engineering and Materials Science

INFLUENCE OF COMPOSITION AND PROCESSING CONDITIONS ON THE MICROSTRUCTURE AND PROPERTIES OF HOT ROLLED MICROALLOYED STEELS

Junyu Duan, M.S.

University of Pittsburgh, 2016

This study investigated the effects of selected chemical compositions and processing conditions on the microstructures and mechanical properties of microalloyed hot rolled band. Also, the comparisons have been made between hot rolled band and QT steel. The microstructures of all the specimens were characterized by optical microscopy, scanning microscopy, electron back-scattered diffraction pattern techniques, and the stored energy was calculated by the subgrain method. The mechanical properties including microhardness, tensile and Charpy V-notch impact properties were measured. The relationship between microstructure and mechanical property behaviors has been made. The results show that vanadium can significantly improve strength at high coiling temperatures, but the effectiveness decreased with the lower coiling temperatures. Vanadium also played a very important role in tempering resistance. The relationship between the relative concentration of vanadium and nitrogen has been discussed. It showed that increasing concentration of nitrogen and decreasing concentration of aluminum would not help to improve the final strength and would increase the grain size.

Coiling temperature is another important parameter in the hot rolling process since the OM, SEM and EBSD results showed that with different coiling temperatures, the microstructures and mechanical properties of the materials exhibited great difference. Influence of Composition and Processing Conditions on the Microstructure and Properties of Hot Rolled Microalloyed Steels Junyu Duan, M.S. University of Pittsburgh, 2016 v The experiment results confirmed the phase transformation predictions made by using the JmatPro thermo-kinetic software.

TABLE OF CONTENTS

LIST OF TABLES

LIST OF FIGURES

ACKNOWLEDGEMENT

It would be impossible for me to accomplish this study without help and kindness from many people. I would like to express my great appreciation to all of them.

At first and foremost, I would like to thank my advisor, Professor Anthony J. DeArdo. His various knowledge and affluent experience in physical metallurgy is always the most important supporting power of my study. I would also thank the other committee members, Professor Mao and Professor Smolinski. Their suggestions and advice have been crucial to completion of this study.

Secondly, I need to thank Professor Hua. He helped me a lot in preparing experiments materials and test specimens, and his ideas are always inspiring and let me think deeper. Special thanks to Dr. Goldman. His help in improving my English speaking and writing skills were a great benefit. I will always remember his smartness and kindness during the last two years.

I also need to thank other BAMPRI members and friends, Dr. Gong, Bing Ma, Petch Janbanjong, Yingjie Wu and Xingchi Feng. They offer me great help in letting me master multiple experimental skills, preparing samples, solving problems in both

academic and non- academic fields, and enriching my leisure time and my life. I will cherish all of your friendship and precious time we have spent together.

I would like to thank BAMPRI (Basic Metals Processing Research Institute) and University of Pittsburgh for providing me necessary experiment facilities and trainings, and thanks to U. S. Steel for providing experimental materials.

Last but not least, I would like to thank my parents, they give me invaluable support to my M.S. program, both the financial support and spirit support. I would also thank my girlfriend, it is her love that accompany me to overcome difficulties, loneliness and bring me infinite happiness as well as courage through all the critical stages.

Thanks all of you very much!

This thesis is dedicated to my parents, my girlfriend, and my grandparents in the heaven.

1.0 INTRODUCTION

High strength low alloy steel is a kind of steel that can have good mechanical properties with small amount additions of microalloying elements and good TMCP. At the same time, they have relatively low concentration of carbon that will provide better ductility, impact toughness and weldability.

The chemical compositions and processing conditions are two crucial factors that control the final microstructures and properties. In perspective of strengthening, the microalloying elements, such as vanadium, niobium or titanium, can provide higher strength through grain refinement, dislocation strengthening or precipitation hardening. Different species and level of addition of microalloying elements can strongly influence the final structure and properties. In addition, so do the thermomechanical processing conditions. For example, reheating and soaking temperatures, rolling reduction and temperature, cooling rate and coiling temperature, as well as other processing parameters can exert great influence on the prior austenite grain size, phase transformation, formation of precipitates and other microstructures features.

In order to achieve better properties of materials, the search for desirable combinations of chemical compositions and processing parameters always attract research interests. In this study, several selected alloying elements and processing conditions of HSLA simulated hot band coils were investigated. The relationship among composition, processing, microstructures and properties were studied.

2.0 BACKGROUND INTRODUCTION

2.1 INTRODUCTION TO THERMOMECHANICAL PROCESSING OF HSLA STEEL

2.1.1 Rough rolling and finish rolling

Thermomechanical processing is a scheduled hot rolling process that applies hot deformation to both change the dimensions and alter the internal microstructures of the steels. One of the goals of hot rolling is to achieve a fine, uniform austenite grain size characterized by high S_v parameters. Immediately after hot rolling, the austenite is cooled to room temperature under highly controlled conditions. Therefore, the deformation stage of the TMP process is also referred to as austenite conditioning. There are two different TMP methods to achieve austenite grain refinement, conventional controlled rolling (CCR) and recrystallized controlled rolling [1].

Austenite with finer grain size can provide more potential nucleation sites for ferrite during the transformation and lead to finer ferrite grain size which is beneficial for both strength and toughness. The density of nucleation sites (prior austenite grain boundaries and deformation bands) can be expressed as the interfacial area of near planar boundary per unit volume S_v with the units mm^{-1}. So, S_v is a good indication of the effectiveness of

the TMP in austenite conditioning. The larger the S_v, the finer the ferrite grain size will be. The relationship between S_v and grain size is indicated below for steels of high transformation temperature and ferrite-pearlite microstructures.

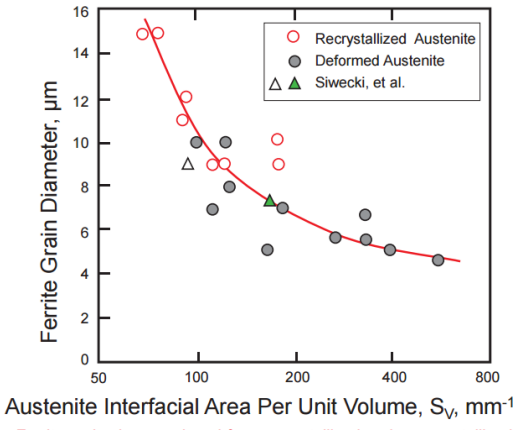

Figure 1. Ferrite grain size produced from recrystallized austenite as various S_v values

Austenite conditioning by TMP occurs as follows: (i) after reheating and rough hot rolling above the T_{95} temperature, there will exist a fine, uniform, equi-axed austenite microstructure; (ii) further substantial deformation will take place below T_5 (the temperature for 5% recrystallization), leading to a pancaked or deformed austenite grain shape. For this approach, the steel remains unrecrystallized during the rolling process below T_5, or in the so-called finishing passes. Therefore, the austenite grains will be severely distorted after deformation, and the deformation bands as well as transgranular twins will occur. This process is called conventional controlled rolling or CCR. A high T_5 is beneficial for CCR to allow more rolling passes to occur between T_5 and finishing temperature. Figure 2 indicates the difference between CCR and RCR.

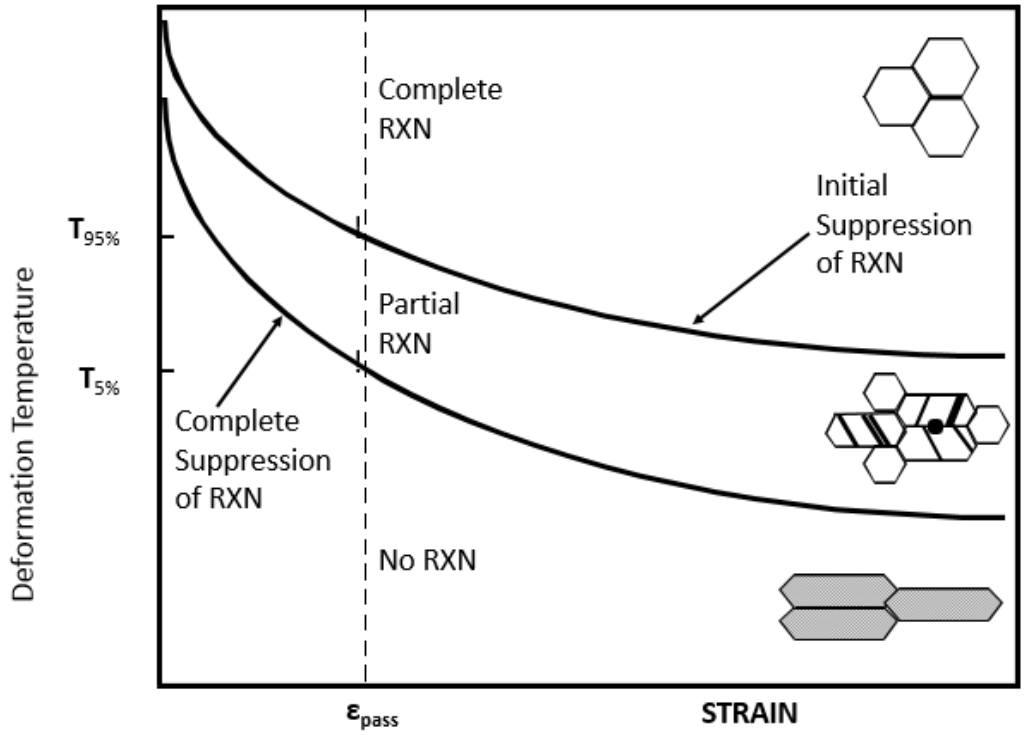

Figure 2. Schematic representation of austenite microstructures resulting from various deformation conditions

In normal cases, RCR and CCR are all necessary for thermomechanical processing of HSLA steels. RCR is usually applied at high temperature (higher than T_{95}) as roughing process. CCR is usually used at relatively low temperature (lower than T_5) as finishing process and it is really crucial. Because without rolling under the T_5, HSLA steel will tend to transform to bainitic structure and toughness will be influenced[2].

2.1.2 Reheating and soaking

In the application of TMP, it is necessary to first reheat the steel to well above A_{c3} temperature to: (i) fully austenitize the as-cast ingot or slab prior to TMP processing, and

(ii) to dissolve the microalloyed precipitates. Different soaking temperature will have dramatic impacts on different microstructure features of final products. These features includes the release of free carbon, growth and coarsening of austenite, ferrite to austenite transformation, dissolution of precipitates and cementites[3]. The schematic effects of reheating temperature on microstructure is shown in Figure 3.

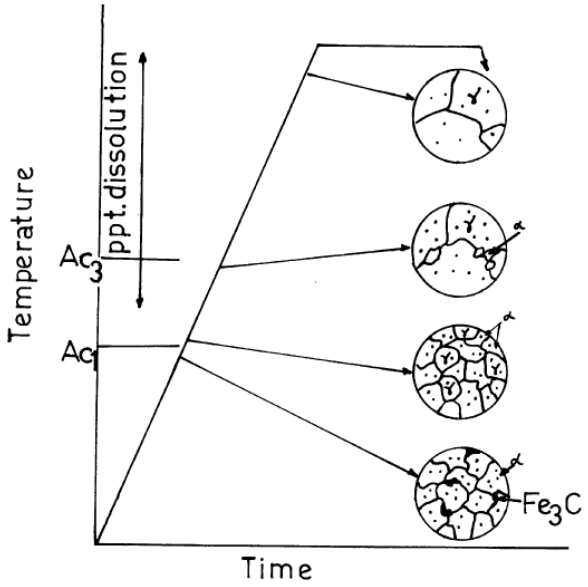

Figure 3. Schematic effect of reheating temperature on microstructure[3]

In microalloyed steels, dissolution and growth kinetics of different carbonitrides is time and temperature dependent. The precipitates which have low solubility product and difficult to dissolve at high temperature could serve as effective grain coarsening inhibitor by their pinning force exerted to the grain boundary. Another important thing is only if the precipitates size is smaller than the certain critical size, the precipitates could be used to refine the grain. When isothermal temperature is greater than the critical value,

significant coarsening of precipitates will take place, and this critical value is called grain coarsening temperature and it is much lower than the dissolution temperature of precipitates[4]. When soaking temperature is lower than grain coarsening temperature, grain growth is suppressed by small precipitates particles, otherwise isolated grains will grow at the expense of surrounding grains. For different microalloyed elements, the grain coarsening temperature (GCT) of their carbonitrides are also different (Figure 4). TiN and Nb(CN) have the relatively high GCT, they can be soaked at high temperature without losing the ability to inhibit grain coarsening, but for vanadium the grain coarsening temperature is much lower.

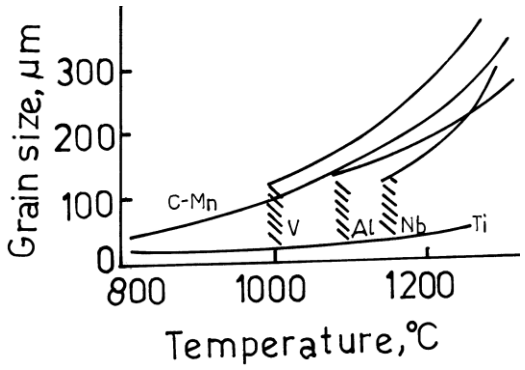

Figure 4. Effect of reheating temperatures on austenite grain size

2.1.3 Cooling

When the products has gone through the finishing rolling, they will undergo accelerated cooling. The purpose to use water cooling after hot rolling is to acquire lower temperature transformation products such as acicular ferrite, bainite and martensite to achieve high strength with lower carbon concentration[5] and refine the grain. Water spray

cooling rates in both strip and plate mills range from 10-40 C/s. The CCT diagram can be used to illustrate the influence of cooling rate to the final phases formed. Figure 5 indicates the phases of HSLA steel formed in different cooling conditions.

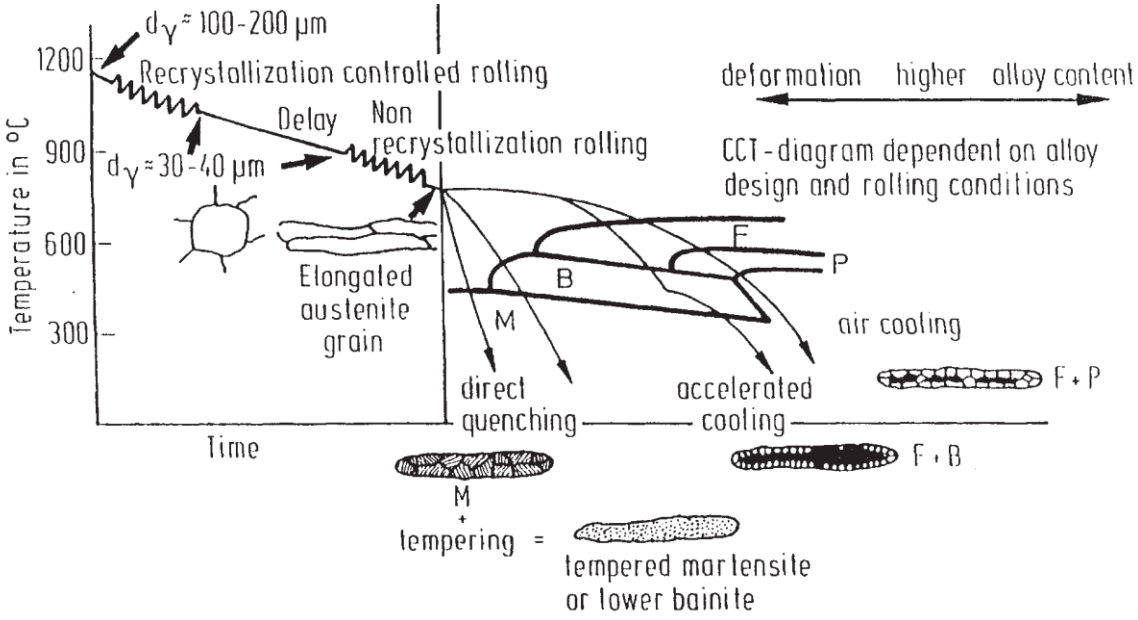

Figure 5. Thermomechanical rolling plus in line cooling of HSLA steels

Apart from the influence to the phases, accelerated cooling has dramatic effects on ferrite grain size, higher cooling rate will lead to smaller ferrite grain. Although this grain refinement effect decreases with increasing cooling rate[6]. Also, higher cooling rate is beneficial for precipitation hardening in microalloyed steel. It promotes finer precipitates' formation[2], and significantly increases the strengthening effectiveness of nitrogen and microalloyed elements. But with increasing cooling rate, the impact toughness of the product is reduced and ductile-brittle transition temperature is also increased because of the enhancement of precipitation strengthening[6].

2.1.4 Coiling

Once the products are cooled to a certain predetermined temperature, the cooling process is stopped and hot strip is gathered or wrapped into a coil[2]. This final process is called coiling, and the in-coil cooling rate is approximately 30C/h. The coiling process has great influence on the final microstructure of HSLA steels. It can be regarded approximately as an isothermal transformation process. Therefore, different phases and morphologies will be formed with different coiling temperatures, and the dislocation densities will also increase with lower coiling temperatures[7]. The variance presented in microstructures caused by changes in coiling temperatures will lead to differences in microstructures and mechanical properties, including strength and toughness. For microalloyed steel, precipitation hardening will also be influenced by coiling temperature. Opinions about effects of coiling temperature to precipitation hardening are varied. Wilson and Gladman found low coiling temperature could help nitrogen remain in solution in hot strip while the low volume fraction of carbonitrides would formed[4]. In lower coiling temperature, strain aging attitudes become higher because larger amount of interstitial elements, such as carbon and nitrogen, are kept in solution[7]. This will result in the reduction of contribution of precipitation hardening to the total strength. But in some other researches, it was reported that lower coiling temperature made contribution to finer size of precipitate by increasing nucleation sites for precipitates because the driving force for precipitates' formation was high at low temperature growth rate of precipitates[8] was low. So the lower coiling temperature will lead to increase of the contribution of precipitation hardening to the total strength. But generally speaking, the hardness and strength will

increase at low coiling temperature because the phases formed in low coiling temperature have higher dislocation densities and are therefore stronger than the ferrite formed at high coiling temperature. The Figure 6 indicates the relationship between coiling temperatures and strength of 2 different microalloyed HSLA steels.

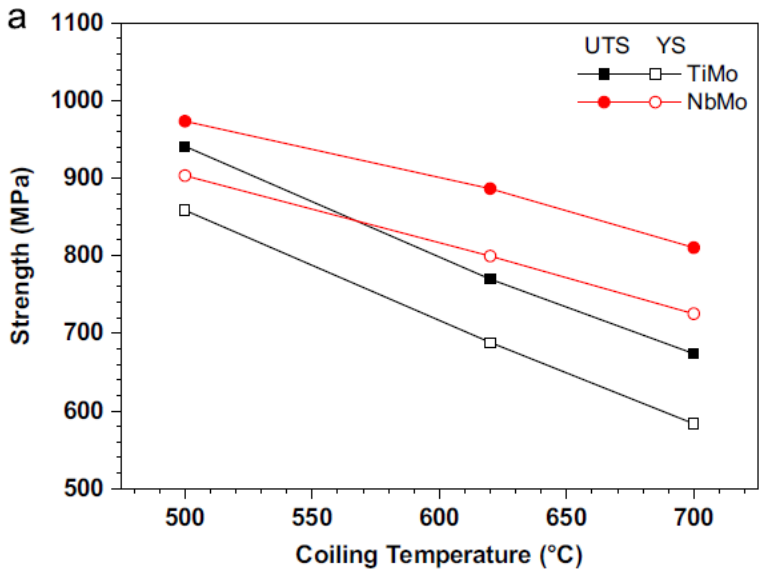

Figure 6. Yield and tensile strength of TiMo and NbMo steels as a function of different coiling temperatures[8]

2.2 INFLUENCE OF CHEMICAL COMPOSITION TO PROPERTIES OF HSLA STEELS

2.2.1 Vanadium

Vanadium is the microalloying element that has been frequently added into steels to improve their properties. It has great influence on the microstructures of modern steel,

including suppression of recrystallization, retardation of grain coarsening, as well as precipitation behaviors.

There is a large difference between vanadium and other microalloying elements such as Titanium and Niobium. At first, the solubility of vanadium itself is the highest among microalloyed elements mentioned before, so it is not easy to precipitate out in austenite. The solubility of vanadium carbonitrides in austenite is also much larger than other ones. But its nitrides' solubility is substantially lower than its carbides'. Figure 7 shows different solubility products of different carbides and nitrides in austenite as a function of temperature.

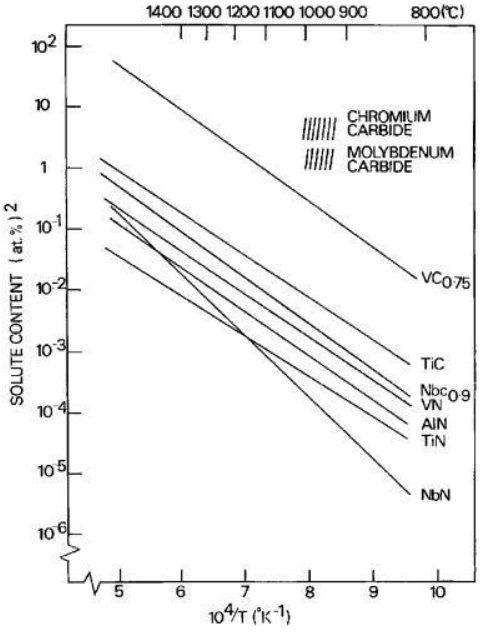

Figure 7. Solubility products, in atomic per cent, of carbides and nitrides in austenite as function of temperature[9]

One of the common characteristic of microalloying elements is that the addition of the elements can increase the recrystallization stop temperature. Through solute drag and particle pinning, the strain induced precipitates can effectively retard the coarsening of the grain and recrystallization process[10]. Figure 8 indicates the effectiveness of different microalloyed elements in increasing the recrystallization stop temperature. It is easy to point out that vanadium is the least effective one. The reason is the solubility product of vanadium carbides is relatively high, so in the temperature range of hot rolling, little strain induced precipitates would form, and it hardly affects the deformation process.

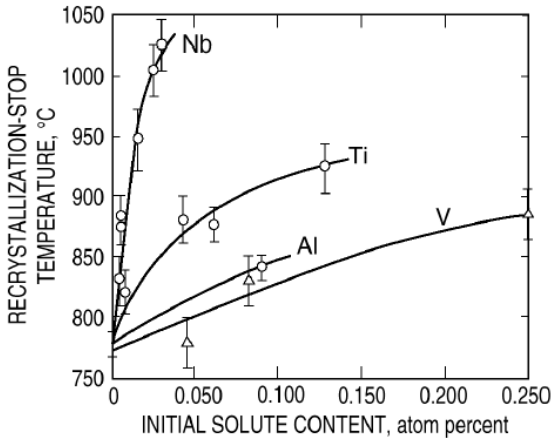

Figure 8. The increase in recrystallization-stop temperature with increase in the level of microallyed solutes[11]

Because of the large gap between the solubility of V(C, N) and VN, it makes vanadium an easy controlled microalloyed element with regard to precipitation strengthening. The amount of nitrogen addition highly influence the degree of precipitation strengthening because it determines the density of V(C, N)[10] by increasing

the driving force of V(C,N)'s formation. Figure 9 indicates the significant increase of particle formation driving force after addition of nitrogen.

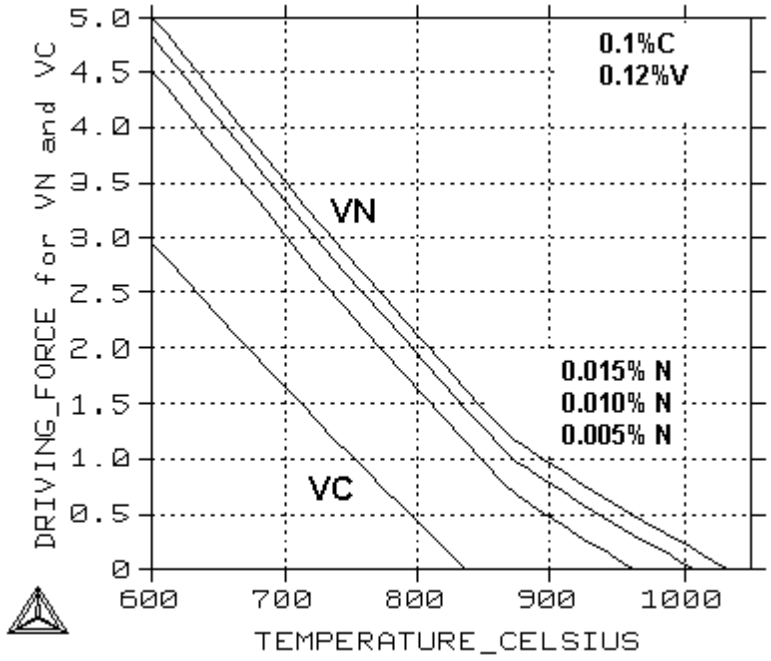

Figure 9 . Chemical driving force, ΔGm/RT, for precipitation of VC and VN in 0.12% V steel.

Just like indicated above, there is very little strain induced precipitation of V(C, N) due to the high solubility product of V(C,N) in austenite. To achieve precipitation strengthening, vanadium must completely dissolve in austenite, combining with interstitial elements and precipitate out as carbides and nitrides in γ/α-transformation process. The formation of precipitates benefits a lot from this transformation process due to the significant increase of chemical driving force and the lower solubility of precipitates in ferritic structure[10]. There are two major mechanisms occur for precipitation in ferrite. For interphase precipitation, precipitates sheets would develop

along the γ/α boundary regularly and repeatedly with regular spacing. For general precipitation, Vanadium carbonitrides could precipitate in ferrite mainly on sub grain boundaries. In the perspective of strengthening, just a modest addition of vanadium could produce substantial increase of strength. It has been confirmed that 0.10% percent addition of V would lead to 250 – 300Mpa strength increase. The observation of the Baker-Nutting orientation relationship between the VCN and the ferrite confirmed by SAED has proved that the most of V(C, N) precipitates formed in ferrite[9].Vanadium's solubility in austenite is large and can be dissolved in a relatively low reheating temperature. This feature is beneficial for ferrite strengthening and RCR. In recrystallized controlled rolling, lower reheating temperature is needed which makes it a more economical way to choose vanadium as microalloyed element.

Because of the precipitation behavior of vanadium carbonitrides described above, it is common to add titanium and vanadium simultaneously into the steel alloy design. Due to the high stability and low solubility of strain induced Ti(C,N), it can be used as a very effective grain coarsening inhibition system. V(C, N) which mainly precipitates out in ferrite acts as ferrite strengthening system[1].

2.2.2 Aluminum Nitrides

Aluminum has strong affinity to oxygen. Due to this special property, it is often added into steel to manufacture the Aluminum-killed steel. Through this method, the porosity can be minimized during both solidification and welding.

Apart from removing the oxygen from alloy system, the precipitation of aluminum nitrides has strong influence on mechanical properties to steels, and its importance is no

less than other microalloyed elements such as vanadium, niobium and titanium, although it is usually not regarded as a micoalloying element[4].

Grain size is one of the most significant microstructure features that control the mechanical properties of steels. Smaller grain size can improve the strength and toughness of steels simultaneously. Although there are some other ways such as rolling and accelerated cooling can be used to refine the grain, but it has been proved that the most economical way to achieve the grain refinement is to choose Al-killed steel[4]. The source of grain refinement in Al-killed steel is AlN particles[4].The solubility of AlN is high at high temperature and will decrease with decreasing temperature. The solubility product, [%Al][%N] is temperature dependent[12], the relationship is indicated as the equation below.

$$\log[\%\mathrm{Al}][\%\mathrm{N}] = \frac{-7400}{T} + 1.95$$

When the solubility product exceeds the solubility limit at a given temperature, precipitation of AlN might occur, if the diffusivity is high enough. Just like other microalloying elements, the dispersion of aluminum nitride particles can effectively retard the growth of grains below the grain coarsening temperature during reheating, and the grain size will markedly increase when temperature is above the grain coarsening temperature. It can be seen from Figure 5 that the solubility product of AlN is between TiN and VN, so the pinning force it exerts to retard coarsening would be expected to be intermediate value between these two nitrides. The relationship between contents of AlN and grain size is shown in Figure 10.

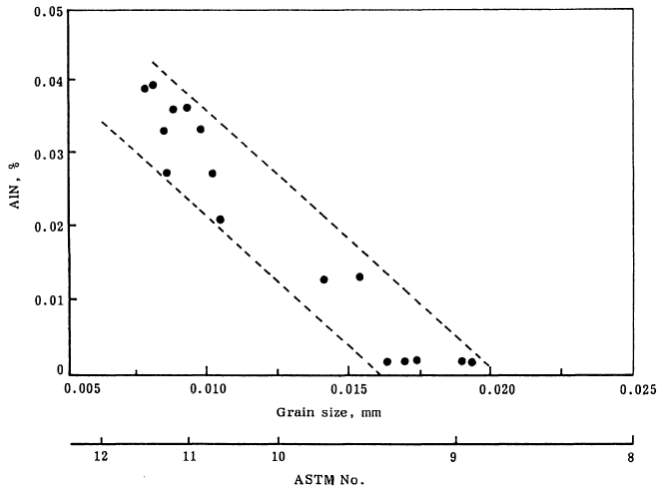

Figure 10. Relationship between AlN contents and grain size in C-Mn steel

2.3 STORED ENERGY FOR HOT ROLLED STEELS AND ITS MEASUREMENTS

Although the major part of mechanical energy released in plastic deformation transfers into heat, the remaining part not converted into heat is the stored energy, which mainly exists in evolving defect structures[13] ,mainly dislocations. Stored energy is the initial driving force for recovery and recrystallization. The defects are present as dislocations and point defects, line defects and planar defects (twins, stacking faults, grain and sub-grain boundaries)[14]. Several studies have indicated that stored energy increases with increasing deformation extent, lowering the deformation temperature and addition of certain alloy elements into pure metals[15–17]. Dislocation density is a good indication of crystal defect density with associated lattice strain, so the increase of dislocation density will be accompanied by increase of stored energy[14].

Compared with cold worked steels which accumulate large stored energy during the deformation process, stored energy of hot rolled steels is much less due to the stored energy originates from the transformation strain and not deformation.

2.3.1 Measurement methods of stored energy

There are several methods to investigate the stored energy. Some common methods are indicated as below.

2.3.1.1 Image quality method The image quality, or pattern quality is determined by electron back scattering patterns (EBSD). The value of image quality is from the grey level corresponds to the maxima and minima of Hough transform[18]. It can be used to calculate the stored energy of deformed steels because of its strong relationship with the amount of lattice defects and internal stresses[18,19]. The stored energy at each lattice site S_i is regarded as proportional to the image quality distribution H_i. The relationship is indicated as equation below.

$$S_i \propto H_i = 10\left[1 - \frac{Q_i(g_i) - Q_{\min}}{Q_{\max} - Q_{\min}}\right]$$

Q_i is the image quality at site i with grain orientation g_i. Q_{max} and Q_{min} are the maximum and minimum image quality of aggregate[18]. However, since the results can be influenced by several experimental factors such as surface quality and beam quality, image quality can only be treated as a semi quantitative value to measure stored energy[14].

A new method put forward by BAMPRI[20] is able to minimize the errors caused by experiment conditions.

2.3.1.2 Subgrain method For the subgrain method put forward by Choi[18], the subgrain structure is used for calculating the stored energy. If the dislocation substructure can be simplified in the form of subgrain of diameter D and boundary energy γ, the geometric constant α~3[21], then the stored energy, Si of each lattice site can be given by:

$$S_i = \alpha \frac{\gamma}{D}$$

The subgrain size and misorientation can be determined by reconstructing the subgrain structure from EBSD data, and only the boundaries with misorientation greater than the critical resolution angles (0.5, 1 and 2◦) are recognized as subgrain boundaries. If the boundry energy of subgrain is only regarded as a function of the boundary misorientation (△θ) and has no relationship with boundary types (tilt and twist), the boundary energy from the Read–Shockley equation[22] can be expressed as the following equation:

$$\gamma(\Delta\theta) = \begin{cases} \gamma_m \dfrac{\theta'}{\theta^*}\left[1 - \ln\left(\dfrac{\theta'}{\theta^*}\right)\right] & \theta' < \theta^* \\ \gamma_m & \theta' \geq \theta \end{cases}$$

where θ’ = |△θ | for $0 \leq |\triangle\theta| \leq \pi$ and θ’ = 2π − |△θ| for $\pi \leq |\triangle\theta| \leq 2\pi$, △θ is the boundary misorientation between two neighboring subgrains, θ∗ is the misorientation limit for low angle grain boundaries, which was chosen as 15°, and γ_m is the specific

energy of high angle grain boundaries. In this study, subgrain method will be used to construct stored energy distribution map and calculate stored energy in different specimens.

2.3.1.3 Taylor's Factor Method For the Taylor's Factor method, the Taylor's factor is theoretically calculated by Taylor's model, and it is the measurement of stored energy[18]. The stored energy of each site, S_i can be regarded as proportional to the Taylor's factor M_i. The relationship can be expressed as the equation below.

$$S_i \propto M_i = \frac{\sum_s |\dot{\gamma}^s|}{d\varepsilon_{\text{eff}}}$$

Where γ_s is the shear strain rate and $d_{\varepsilon\text{eff}}$ indicates the von Mises strain increment. But the TF method cannot provide the severe inhomogeneous distribution of stored energy in the deformed grains after cold rolling. That is the reason why TF method cannot be used for evaluating stored energy in deformed grains after cold rolling.

2.4 STRENGTHENING MECHANISMS OF STEELS

For hot rolled microalloyed steels, the major strengthening mechanisms include grain size and dislocation strengthening, solid solution strengthening and precipitation strengthening. Each mechanism will be discussed as below.

2.4.1 Grain size and dislocation strengthening

Grain size strengthening, or grain boundary strengthening is a strengthening method by changing the average grain size of the crystalline materials. The theoretical base for this method is that the grain boundary can effectively impede the movements of dislocations. According to Hall and Petch, the dislocation pile-up occurs at grain boundary thereby causing the concentration of the stress. The Hall – Petch equation revealed the relationship between grain size and yield strength[23]. The equation is indicated as below.

$$\sigma_y = \sigma_0 + k_1 D_{GB}^{-1/2}$$

In this equation, D_{GB} refers to the grain size, and σ_0 and k_1 are constants. σ_0 is the strength comes from friction stress which includes contribution from solutes and particles. $K_1 D_{GB}^{-1/2}$ can be regarded as the strength comes from the presence of grain boundary.[24]

When the material is deformed, the Hall-Petch equation can be written as[25]:

$$\sigma(\varepsilon) = \sigma_0(\varepsilon) + k_1(\varepsilon) D_{GB}^{-1/2}$$

Where $\sigma_0(\varepsilon)$ and $k_1(\varepsilon)$ are constants when the material is under certain strain. $\sigma_0(\varepsilon)$ is the constant which is independent of high angle grain boundary (HAB), and it is related to dislocation density accumulated at the dislocation boundaries or the low angle grain boundaries (LAB). Approximation of dislocation density of a mixed tilt/twist boundary can be written as $1.5 S_v\theta/b$, where S_v is the area of boundaries per unit volume, θ is the

misorientation angle and b is the Burgers vector. In this case, the Hall-Petch equation can be written as:

$$\sigma_f = \sigma_0 + M\alpha G\sqrt{1.5b(S_V\theta)_{LAB}} + k_1(\varepsilon)D_{HAB}^{-1/2}$$

Where σ_0 is the frictional stress, M is the Taylor factor, α is a number and G is the shear modulus. It can be known from this equation that flow stress analysis of deformed metal is complex. The substructures of the material are mixed, and show different resistances to slip because of the misorientation changes of low angle grain boundaries[24].

The analysis above shows that both dislocation strengthening (low angle grain boundary strengthening) and grain size strengthening (high angle grain boundary strengthening) are important to yield strength of deformed metals. The structural parameters of both cases should be taken into account when Hall-Petch equation is being applied.

2.4.2 Solid solution strengthening

There are two types of solid solutions in steels, interstitial solid solutions and substitutional solid solutions[26]. The elements which have similar size and electronic structure with iron and do not combine with other elements to form carbides and nitrides, and just replace the positions of iron atoms in bcc ferrite or fcc austenite structures are substitutional solid solutions[12]. The differences of size and electronic structures between substitutional solute atoms and iron have strong effects over lattice parameters of unit cell, the modulus of elasticity, and the shear modulus of the ferrite[27]. The atoms that are small enough to dissolve in the interstitial sites of ferrite or austenite structure, such as

carbon, nitrogen and boron, are interstitial solid solutions. The schematic illustration of these two types of solid solutions are indicated as below.

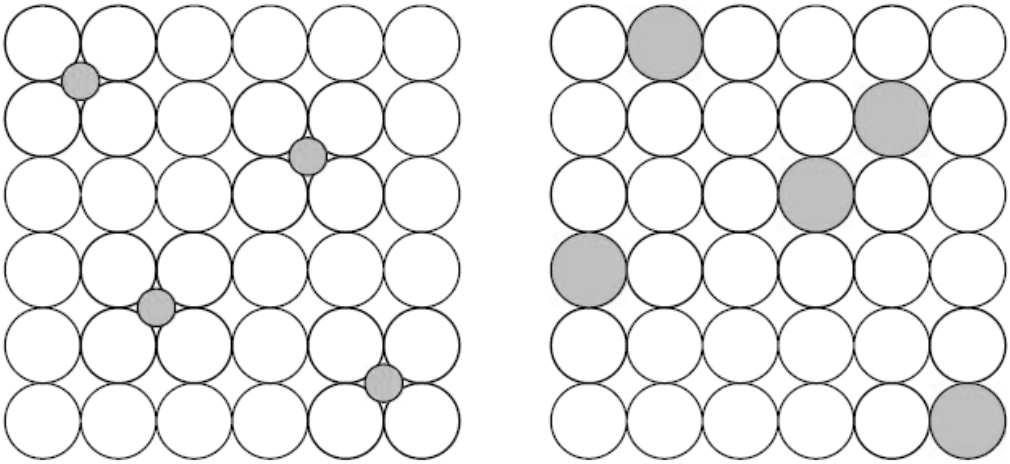

Figure 11. Schematic illustration of an interstitial solid solution (left) and a substitutional solid solution (right)[26]

The increase of strength of solid solution strengthening comes from the interaction between stress field caused by the introduction of solid solution elements and the dislocations. The substitutional solid solutions just provide the modest solid solution strengthening. On the other hand, the interstitial elements make significant contributions to solid solution strengthening. But they are easy to segregate at the dislocations or to form precipitates as carbides or nitrides. The relationship between the increase of yield strength to the addition of solid solution elements is indicated in Figure 12.

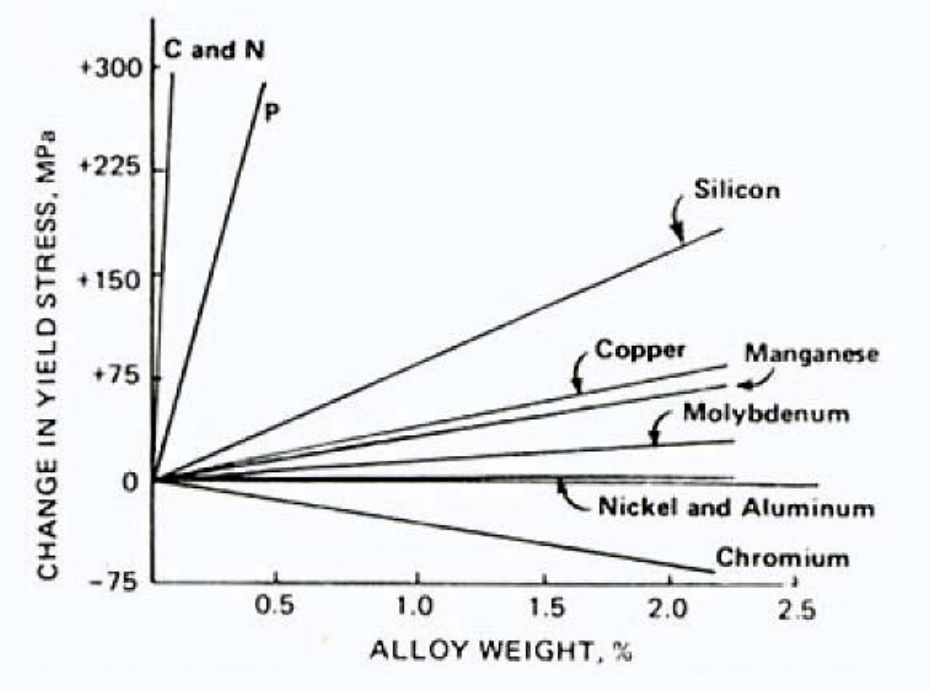

Figure 12. Solid solution strengthening of ferrite as a function of alloying element content low carbon steels[28]

From Figure 12, it is easy to see that there is a linear relationship between alloy weight and increase of yield strength, and this relationship is applicable for both the substitutional and the interstitial solid solution strengthening. It can be written as the equation below[29]:

$$\Delta\sigma_{ys\ (SS)} = \Sigma\ (\chi_i k_i)$$

In this equation, χ_i refers to weight fraction and k_i refers to the strengthening coefficient of each alloy element. The total strength contribution equals to the sum of the product of χi and k_i.

2.4.3 Precipitation strengthening

The precipitation hardening mainly relies on the second phase particles. The movements of dislocations can be impeded by these tiny particles. In deformed metals which contain second phase particles, the balance of forces acting during particle resistance to dislocation movement is shown schematically in Figure 10[30]

Figure 13. Balance of forces acting during particle resistance to dislocation movement

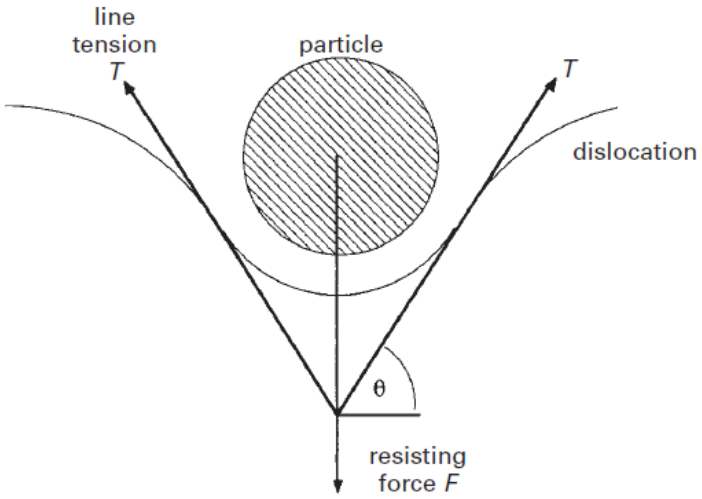

Figure 13. Balance of forces acting during particle resistance to dislocation movement

According to force balance, the relationship between line tension and resisting Force can be written as:

$F = 2T\sin\theta$

When $\sin\theta = 1$, the F reaches its maximum value 2T. On the other hand, if the particle is hard, resistance force can be larger than 2T. In this case, the dislocation will bypass either by Orowan looping or cross-slip and the particle will remain non-deformed (shown in Figure 14).

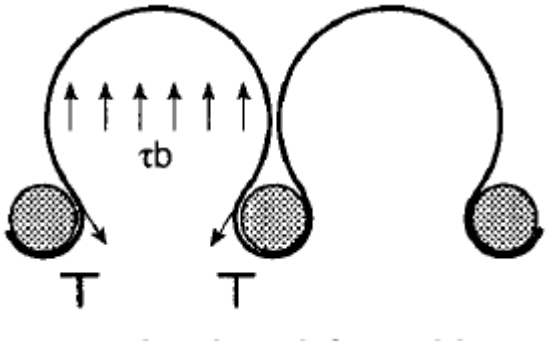

Figure 14. Dislocations bypassing the undeformable second phase particles

According to Orowan relationship put forward by Orowan[31] and Ashby[32]:

$$\Delta\sigma_y = (0{\cdot}538Gbf^{1/2}/X)\ \ln(X/2b)$$

In this equation, the left side is increase of strength due to the addition of second phase particles. G is shear modulus, b is Burgers vector, X is the diameter of the particle, f is the volume fraction of the particles. From this equation it is easy to see that the particle dispersion strengthening effects will be enhanced by increasing volume fraction of particles and decreasing particle diameters. The experiments data match well with the predicted value by Orowan-Ashby equation[30].

If the particles are soft, they will be sheared by dislocation as Figure 15.

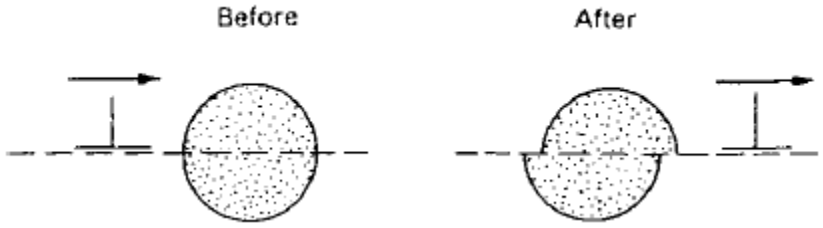

Figure 15. Dislocation motion continue through second phase particles (particle cutting)

In this occasion, the deformation of the particle will lead to increase of the interfacial energy between particles and matrix. Also, the passage of dislocation through the particles might produce an anti-phase boundary with disordering energy or stacking faults energy[30]. The increase of strength due to the change of energy is termed chemical hardening.

A more important strengthening mechanism when particle cutting occurs is coherency strain hardening. The displacements related to interaction between dislocation and strain field of precipitates will produce larger strengthening effects than precipitates along. The dislocation line will bend to lower energy position of strain field, so any applied force need to overcome more obstacles. For smaller particles, the bending of dislocation is limited, but for larger particles, dislocation will have to overcome a larger number of obstacles per unit length to move. In this case, coherency strain strengthening will increase with increasing size of small particles but will decrease with increasing size of larger particles, this trend is shown in figure 12.

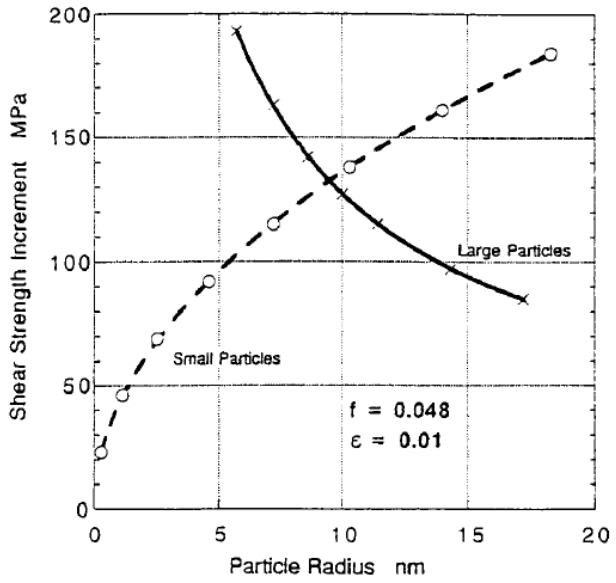

Figure 16. Coherency strengthening effects with regard to particle radius

The Figure 16 indicates the relationship between strengthening effects and size of precipitates. When particles are very fine, the shear strength in the slip plane increases with increasing size for coherency strain hardening. When the size of the particles exceeds the critical value, the strengthening mechanism will change into "large particle mode" as mentioned before or Ashby-Orowan looping model that the strengthening effects will decrease with increasing particle size. Carbides and nitrides in steel follow Orowan-Ashby shown by the large particle branch.

3.0 STATEMENT OF OBJECTIVES

This study is to investigate effects of coiling temperature and chemical composition on mechanical properties of hot rolled band. In order to relate the properties to internal microstructures, several characterization methods were used. Also, the computer-based simulation was conducted to simulate the phase transformation process.

At first, in order to get the raw data to compare the effects of addition of different alloy elements and different coiling temperatures, mechanical properties which include microhardness, ultimate strength and yield strength, impact toughness at given temperature of steels with different grades are measured. The difference of properties are discussed.

The second objective is to understand the internal relationship between properties and microstructures of these steels. To achieve that, comprehensive and systematic microstructure characterizations were conducted which includes optical microscopy, electron microscopy, and various results from electron back-scatter diffraction patterns.

The final part is to develop an understanding about phase transformation under different coiling temperatures. A computer based simulation was performed. The simulation result would be great help to understand the formation of different microstructures during the phase transformation.

4.0 EXPERIMENTAL PROCEDURES

4.1 MATERIALS

The materials for this study are listed in Table 1. The composition difference can be divided into three parts. At first, for steels designated with A, the vanadium concentration is low. For those designated with B, the vanadium concentration is relatively high. Secondly, compared with 2 and 4 series steels, 3 series steels have higher concentration of nitrogen and lower concentration of aluminum. At last, the composition of 4 series steels is very lean, the concentration of alloy elements (Cr and Mo) are very low compared with 2 and 3 series.

Table 1. Chemical composition of steels used in this study

	2A	2B	3A	3B	4A	4B
C	0.097	0.094	0.103	0.102	0.103	0.096
Mn	1.805	1.795	1.780	1.769	1.803	1.772
P	0.010	0.010	0.009	0.009	0.009	0.009
S	0.0019	0.0016	0.0018	0.0019	0.0021	0.0019
Si	0.399	0.395	0.402	0.400	0.405	0.402
Cr	0.505	0.501	0.512	0.509	0.253	0.252
Mo	0.305	0.303	0.307	0.307	0.103	0.102
V	0.0019	0.058	0.0019	0.061	0.0013	0.056
Al	0.027	0.026	0.0032	0.0045	0.026	0.027
N	0.0071	0.0064	0.0095	0.0081	0.0060	0.0055

4.2 THERMOMECHANICAL PROCESSING PATH

The thermomechanical processing of the steels in this study was on a pilot scale hot rolling mill fitted with water spray cooling and coiling capabilities. All of the samples came from laboratory vacuum melted ingots.. The hot rolling procedures are shown as follows:

(1) All the samples were heated to 1250C and soak for 2 minutes

(2) Samples were cooled to rough rolling temperature and deformed then air cooled to room temperature

(3) Heat every sample to 1250C and soaking for 2 minutes again

(4) Samples were cooled and deformed to the finish rolling temperature of 921C with five passes of 27.5% reduction

There are two processing paths after finish rolling, one was cooling to predetermined different coiling temperatures and coiling, or the second was direct quenching and tempering to 600C and soaking for 1 hour, then air cooled to room temperature. For the former path, the three different coiling temperatures were 675C℃ (1C), 575℃ (2C), 500℃ (3C). The later path was regarded as control group in this study (4C). The schematic diagram of the process described above is shown in Figure 17.

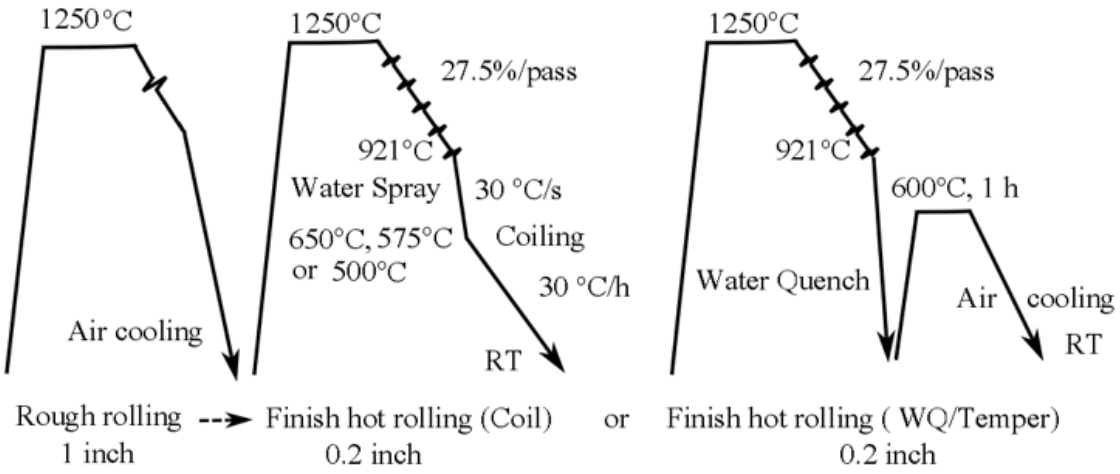

Figure 17. Schematic of thermomechanical processing path

For each grade of steels in this study, the chemical composition or processing parameters are different. A special designation method is shown in Table 2 and Table 3 to represent different samples.

Table 2. Chemical composition designation method

	2x	3x	4x
Cr, Mo concentration	High	High	Low
Al/N	High	Low	High

If x=A, vanadium concentration is low. If x = B, V concentration is high

Table 3. Processing parameter designation method

	Coiling temperature
1C	675C
2C	575C
3C	500C
4C	Water quench/Temper

4.3 EQUIPMENT AND TECHNIQUE

4.3.1 Optical Microscopy

The optical microscopy was mainly used for observing the microstructures of different samples. Samples were cut by Buehler Isomet 1000 diamond cutting saw and hot mounted by copper powder. The silicon carbide abrasive papers range from 400 -1200 grit were used for grinding the samples. After grinding, samples were polished with 0.05 micron alumina power on polishing cloths by electronic Vibratory Polisher. All the samples were etched by 2% Nital solutions for about 10-15 seconds depending on the microstructures of the samples. Optical micrographic images were captured using a Sony digital camera attached to a Nikon Microscope. Two image analytical software, Bioquant and ImageJ were used for analyzing the grain size and volume fraction of microconstituent.

4.3.2 Electron backscatter diffraction

In order to get the more details about microstructures of the samples, especially to obtain the more information about stored energy, EBSD analysis was performed on all the samples. Electron backscatter diffraction is a microstructural characterization technique attached to the scanning electron microscope (SEM) used to study crystalline materials. The samples used in OM analysis were not good enough for EBSD, but needed to be further ground and polished again. In this case, the polishing time ranging from 2 – 5 hours depending on surface condition. The goal of polishing is to eliminate the surface scratches as much as possible and not destroy the surface of samples at the mean time. The standard EBSD operation procedure was applied in this study. The voltage is 20KV and the spot size was 5 corresponding to a beam diameter of 0.5 microns. A step size of 0.2 microns was applied for all observations. A square scanning mode was chosen in order to be compatible with the software used for calculating stored energy distribution. The TSL (EDAX) orientation imaging microscopy (OIM) data collector software was applied for collecting all the data. TSL OIM Analysis software was used for general analysis about grain boundaries and subgrain boundaries, and information about textures and grain orientation could also be obtained from the software. Another important function of TSL OIM Analysis software in this study is to clean up the data after it was collected in order to reduce unnecessary error when the data was transferred to stored energy calculation software.

4.3.3 Transmission Electron Microscopy

Transmission electron microscope (TEM) JEOL200CX was used and operated at 200kv in this study in order to detect and characterize the precipitates generated due to the addition of vanadium and other alloy elements. The preparation of process of the thin foil samples included sectioning the hot rolled strips by diamond saw to about 1mm thick and mechanical grinding the strips on grit silicon carbide papers (600 or 1200 grit), eventually the thickness of the thin foils should be reduced to less than 100μm. Then, the foils were punched to the small discs with 3mm diameters. Finally, these discs were chemically thinned and electropolished using a Fischione twinjet electropolisher (model 110) until the perforation. The electrolyte solution is the mixture of 80g Na2CrO3 and 400ml Acetic acid used at -20C and 40 volts.

4.3.4 Microhardness and tensile test

Microhardness is one of the most significant mechanical properties of materials and has a strong relationship with the strength. The change of microhardness of steels reflected the change of microstructure. The test was performed on a Leco M-400 G microhardness tester and a 300 grams load was chosen. The loading time was set for 10 seconds. Indention size was measured by Bioquant software.

Interstitial elements, such as carbon and nitrogen, play a very important role in the yielding behavior of steels. If the concentration of interstitial elements is high, and the dislocation density is low, yield point elongation will occur. In the stress-strain curve, a

Luder's extension will exist. When YPE happens, the strength of steels will increase and the ductility will decrease. The reason is that the interstitial elements pin at the dislocations and retard their movements. In order to observe whether this phenomenon would occur, tensile test was performed on all materials. The operation procedures followed the ASTM (E8) standards. Duplicate tests were performed on each condition using the MTS electro-mechanic universal testing machine (model 880). The stress-strain curve was automatically plotted by computer.

4.3.5 Charpy V-Notch impact test

Charpy impact toughness is an important mechanical property of steels. It helps to indicate whether the steel has behaved in a brittle manner or ductile manner. This test was govern by ASTM E23. In this study, in order to gain an understanding about the influence of certain chemical composition and processing conditions on fracture behavior, Charpy V- Notch tests were performed.

Before the experiments the Charpy test specimens needed to be specifically prepared[33]. Charpy test bar has a square cross section and contains a notch at the center of its length. When test was conducted, the specimens needed to be supported in a horizontal position. The load is applied by the impact of a heavy swinging hammer at the middle of the beam at the opposite side from the notch, and the specimens were forced to bend and fracture at certain strain rate. In this study, the experiments were performed at 0 ℃. Figure 18 indicates the Charpy bar and the swinging hammer[34].

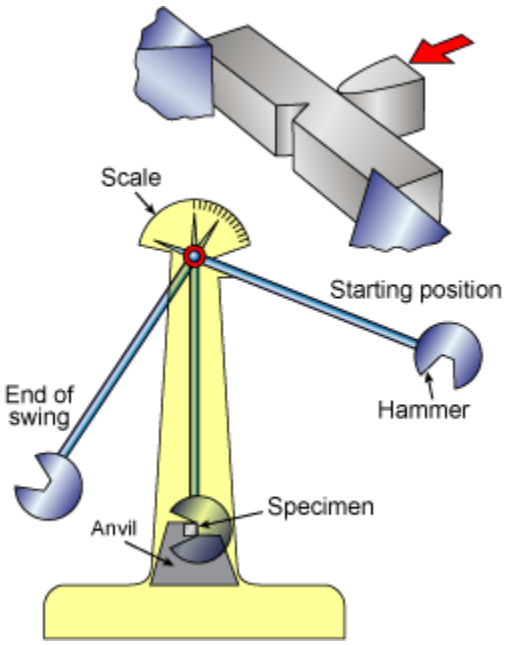

Figure 18. Sketch of the method loading in Charpy test

The response of the impact test is measured by the change of potential energy of the hammer. This energy was then converted into the energy absorbed in fracturing the specimen.

5.0 RESULTS

Figures 19 –21 indicate the microstructures of all steels under optical microscopy. The thermomechanical processing conditions had dramatic effects on the final microstructures of the steels. At high coiling temperatures, polygonal ferrite and pearlite were the main microconstituents. At lower coiling temperatures, non-polygonal ferrite and bainitic ferrite became the dominant phases. This can be further observed by EBSD inverse pole figure.

From the OM figures, the vanadium addition did not have great influence on the morphologies of the microstructures. Under the same processing conditions, the OM images of the same series steels were similar to each other. For grain size, the situation is different. Table 4 shows the ferrite grain size of different series steels at high coiling temperature. For series 2 and 3 steels, the addition of vanadium did not refine the grain structures, in fact, the grain size of the steels with the vanadium addition was even coarser. For series 4 steels, the situation was a little bit different, in that the grain size of 4B was slightly smaller than 4A. The relative concentrations of Cr, Mo, Al and N had more significant influence on the grain size. The ferrite grain of 3 series steels (high N, low Al) was much coarser than 2 series steels (high Al, low N). At the meantime, the Grain of 4 series steels with low Cr and Mo concentration was the coarsest. The data in table 4 confirmed these comments.

Table 4. Ferrite grain size at high coiling temperature

Steel grades	**Grain Size**	**Steel grades**	**Grain Size**
2A1C	7.85	**2B1C**	8.56
3A1C	9.77	**3B1C**	10.57
4A1C	11.83	**4B1C**	10.81

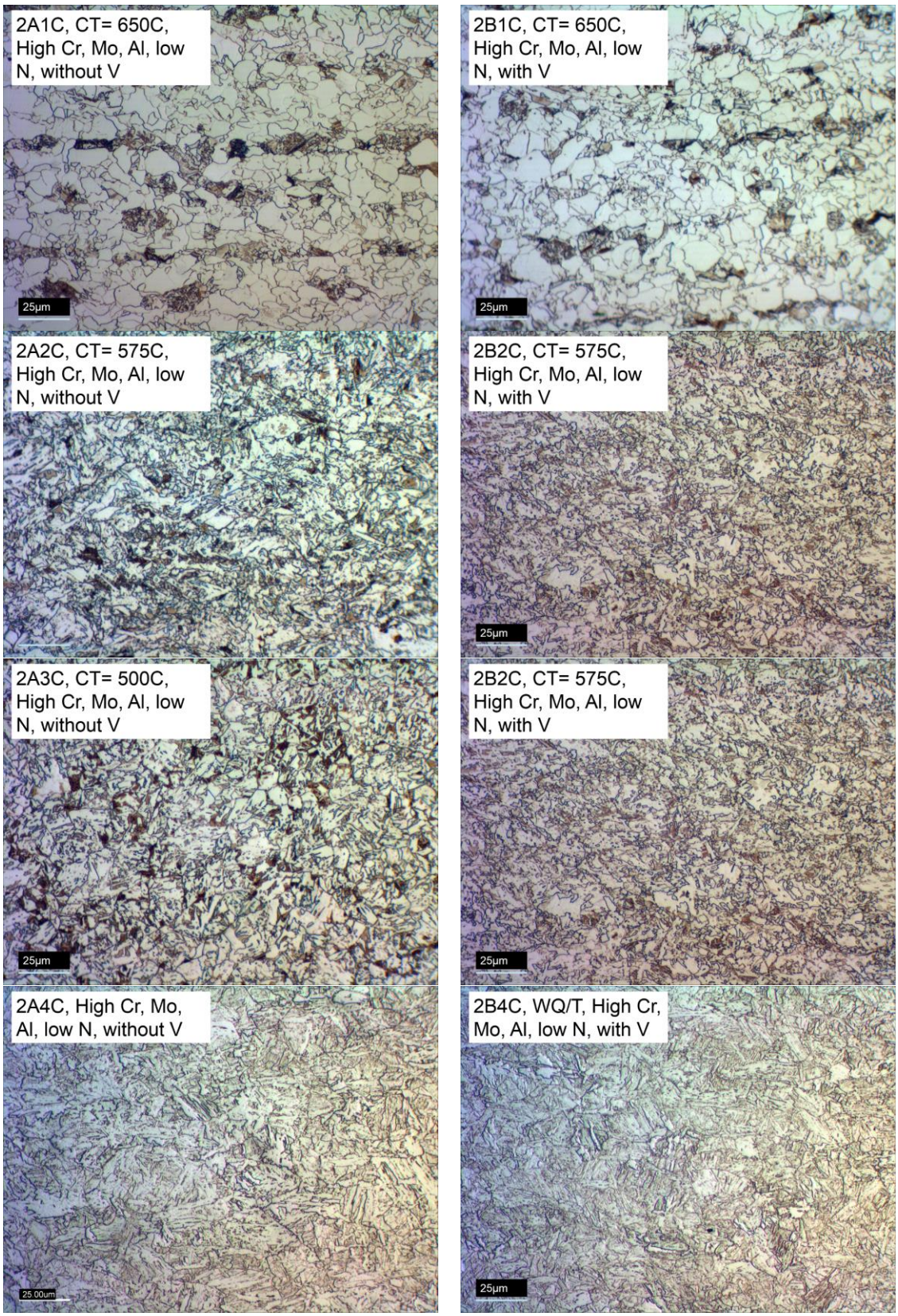

Figure 19. OM images of steels of 2 series

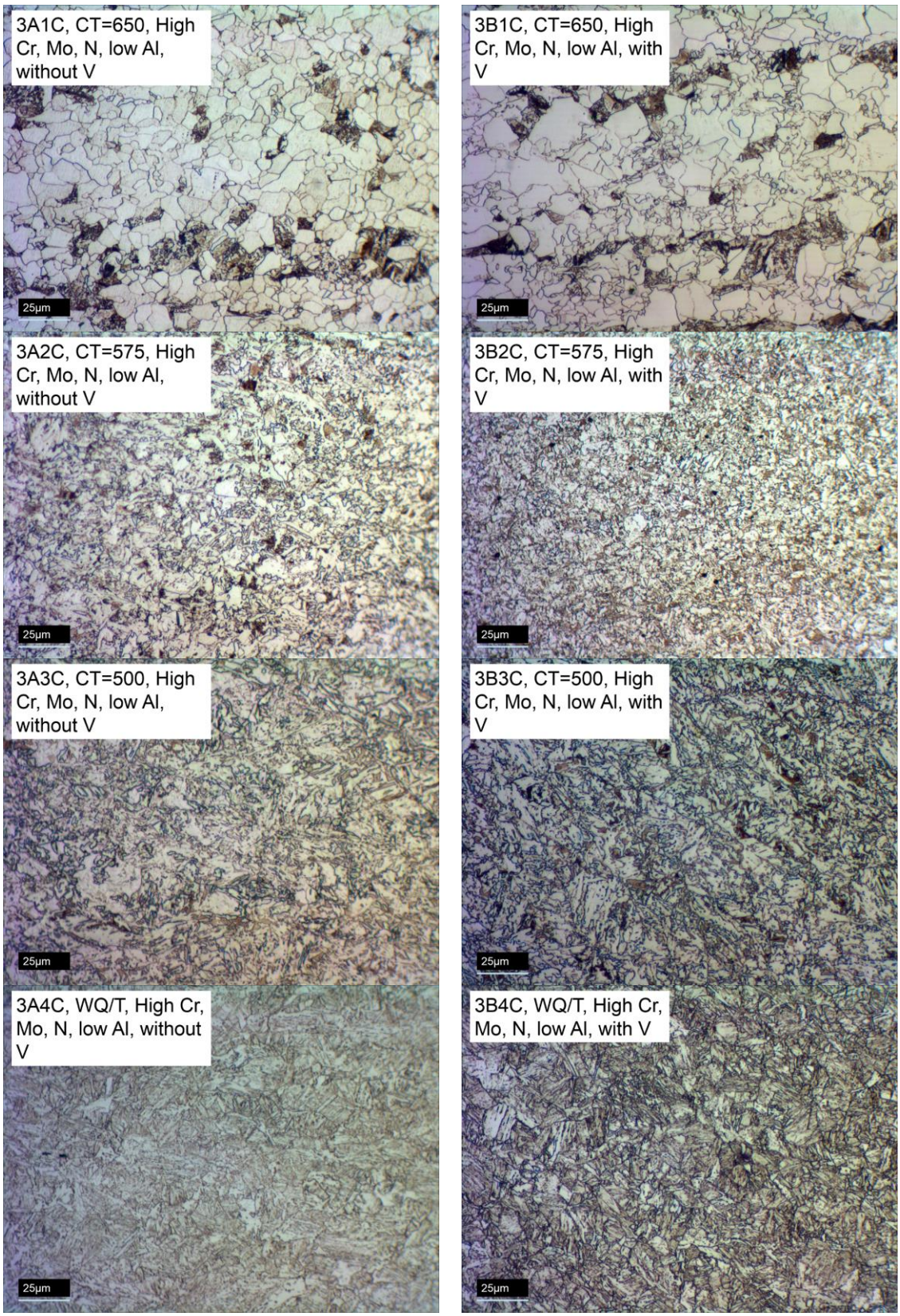

Figure 20. OM images of steels of 3 series

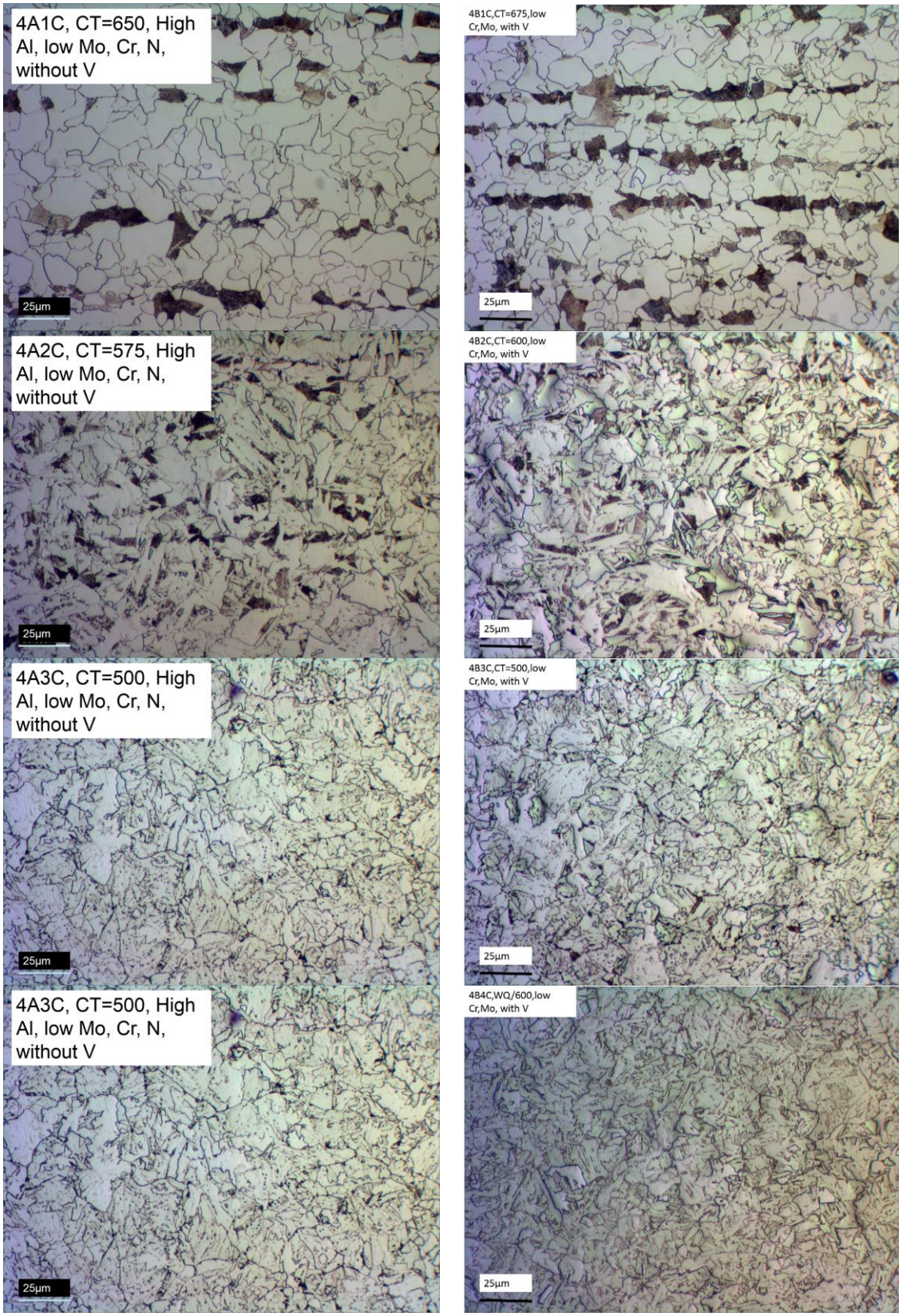

Figure 21. OM images of steels of 4 series steels

Table 5. Microhardness values of all grades of steels

Steel grades	Microhardness	Steel grades	Microhardness	Δ Hardness
2A1C	178 ±5	**2B1C**	210 ±3	32
2A2C	257 ±5	**2B2C**	266 ±4	9
2A3C	282 ±8	**2B3C**	278 ±6	-4
2A4C	254 ±4	**2B4C**	312 ±10	58
3A1C	178 ±11	**3B1C**	215 ±7	37
3A2C	243 ±12	**3B2C**	264 ±2	21
3A3C	263 ±6	**3B3C**	264 ±5	1
3A4C	288 ±4	**3B4C**	335 ±8	47
4A1C	147 ±2	**4B1C**	188 ±8	41
4A2C	189 ±8	**4B2C**	204 ±2	15
4A3C	214 ±6	**4B3C**	226 ±7	12
4A4C	223 ±9	**4B4C**	246 ±3	23

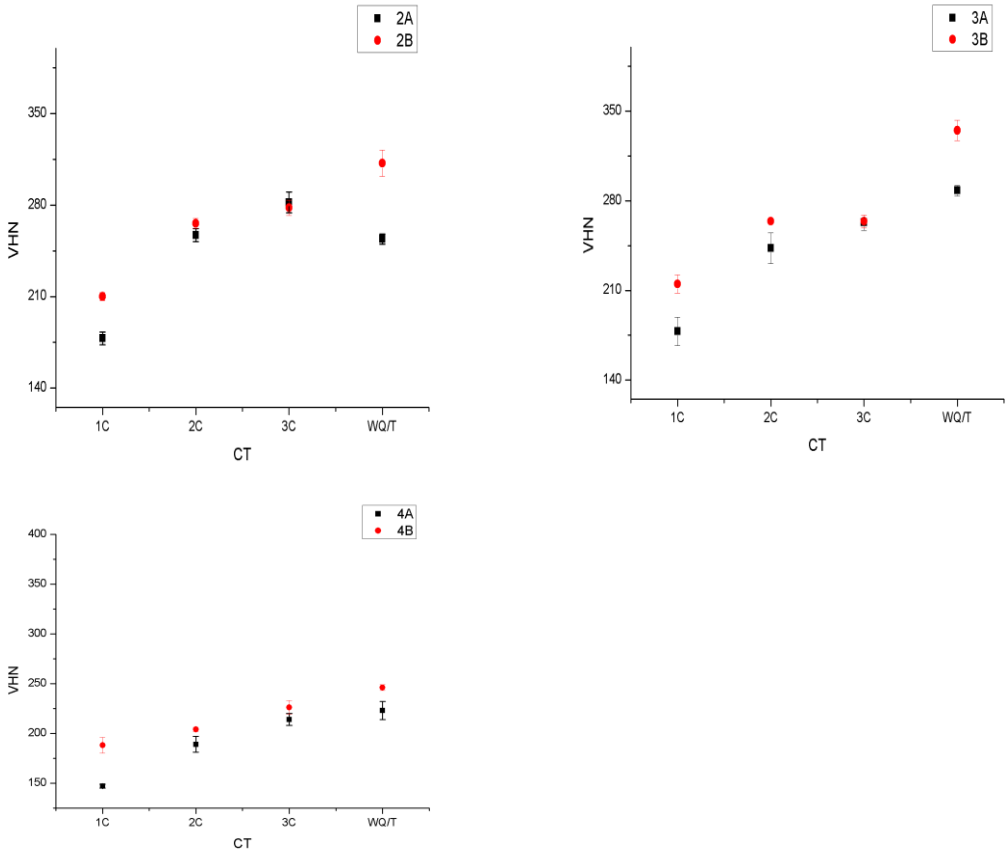

Figure 22. Microhardness of materials with or without the addition of vanadium

Figure 22 shows the effects of addition of vanadium to the microhardness of steels. In series 2 and 4 steels (high Al and low N concentration), the effects of the vanadium addition show the similar changing trends with the change of coiling temperatures. At high coiling temperature, vanadium significantly increases the microhardess of steels, but with the lower coiling temperature, the increase of hardness becomes less and less. At the same time, for water quenching and tempering steels, vanadium addition still effectively increase the tempering resistance. The microhardness of the QT steels with vanadium addition is much higher than those without vanadium addition.

Apart from addition of vanadium, the microhardness of all grades of steels increased with lowering coiling temperature, and the steels which underwent quenching and tempering have the highest hardness values. Another thing needs to be noticed is the most significant increase of hardness occurred when the hardness of the highest coiling temperature was compared to the intermediate coiling temperature (1C to 2C). But when coiling temperature changed from the intermediate to the lowest ones, the increase of microhardness is not as obvious as the previous case.

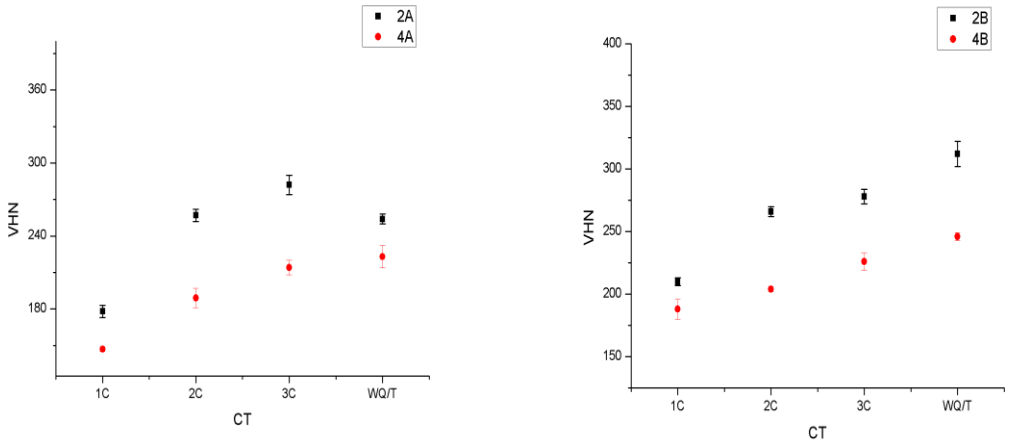

Figure 23. Comparison of microhardness among the steels with high or low concentration of Cr and Mo

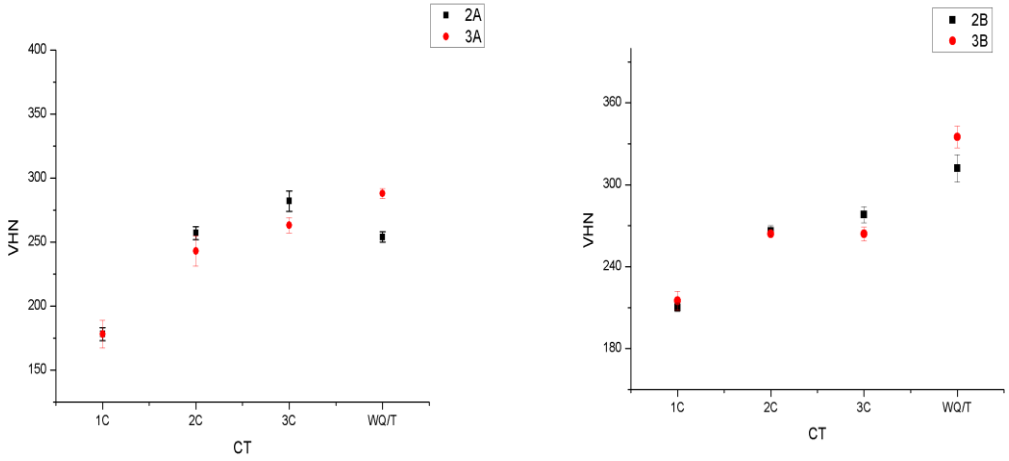

Figure 24. Comparison of microhardness among the steels with high N low Al concentration or high Al low N concentration

Figure 23 illustrates the effects of concentration of Cr and Mo to the microhardness of steels. It is easy to see that under all processing conditions, either in different coiling temperatures or in quenching and tempering, the hardness of 2 series steels(high Cr, Mo concentration) is dramatically higher than 4 series steel.

Figure 24 indicates the influence of the relative concentration of aluminum and nitrogen to the microhardness. The high N and low Al concentration does not lead to increase of hardness after cooling and coiling. At high coiling temperature, the microhardness between 2 series and 3 series steels are almost the same. At the medium and low coiling temperature, the hardness of 2 series steels (high Al, low N) are even higher than 3 series steels (high N, low Al). But in quenching and tempering steel, high N and low Al composition leads to higher microhardness. These effects will be discussed and explained in the following chapters.

Table 6. Strength values of all grades of steels

Steel grades	**Microhardness**	**Steel grades**	**Microhardness**	**Δ Hardness (V steels – V=0 steels)**
2A1C	469	**2B1C**	579	110
2A2C	616	**2B2C**	638	22
2A3C	651	**2B3C**	660	9
2A4C	789	**2B4C**	921	132
3A1C	422	**3B1C**	519	97
3A2C	557	**3B2C**	623	66
3A3C	610	**3B3C**	643	33
3A4C	710	**3B4C**	883	134
4A1C	477	**4B1C**	514	37
4A2C	514	**4B2C**	575	61
4A3C	569	**4B3C**	617	48
4A4C	628	**4B4C**	674	46

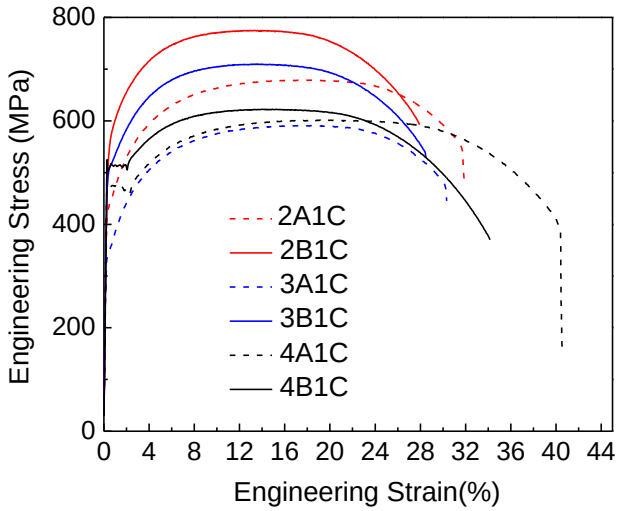

Figure 25. Strain–Stress Curves of hot band steels with high coiling temperature CT=650

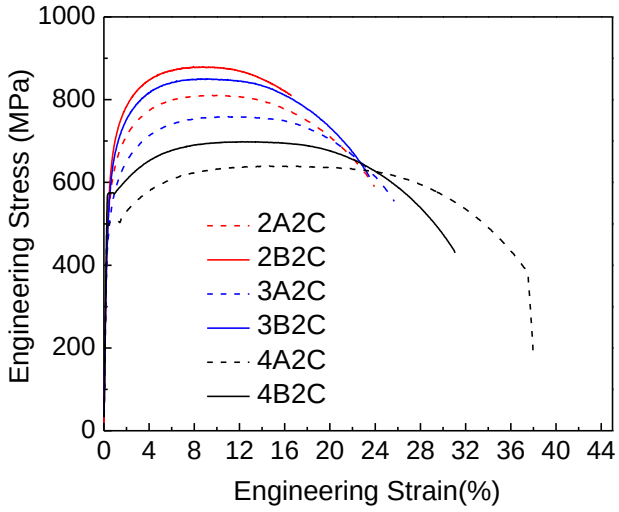

Figure 26. Strain–Stress Curves of hot band steels with intermediate coiling temperature CT=575

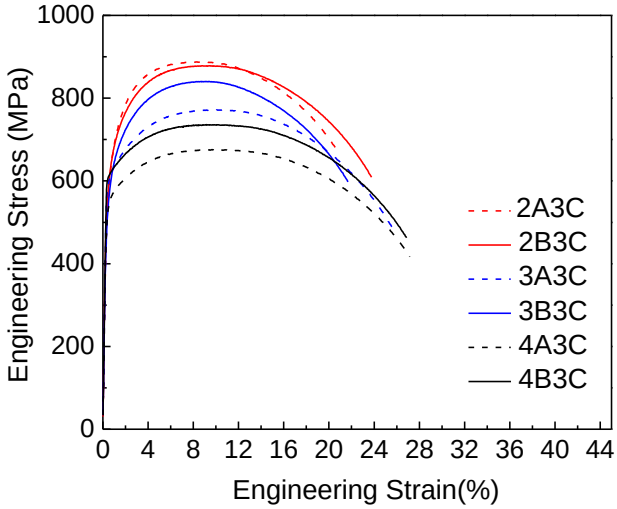

Figure 27. Strain–Stress Curves of hot band steels with low coiling temperature CT=500

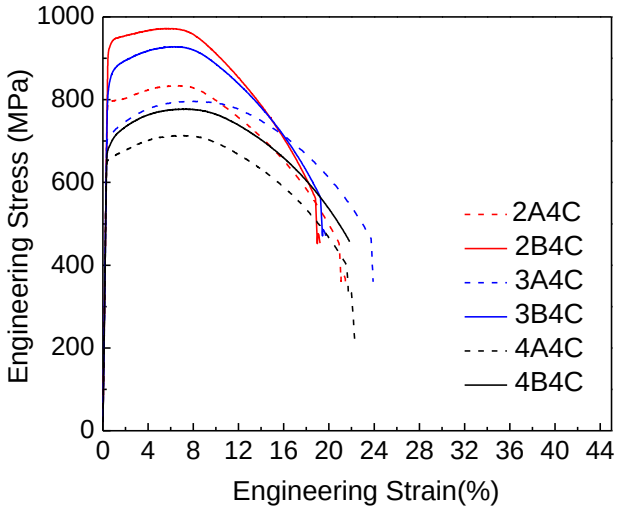

Figure 28. Strain–Stress Curves of quenching and tempering steels

Table 6 indicates the results of yield strength and increase of yield strength due to the addition of vanadium. It shows almost the same trend as microhardness. Yield

strength increased with decreasing coiling temperature, and effectiveness of vanadium addition decreased with lower coiling temperature.

Figure 25-28 are engineering stress-strain curves of the steels under different processing conditions. It is clear that increasing strength would sacrifice the ductility. Higher strength would lead to decrease of the elongation before fracture happened. For 4 series steels (lean composition), yield point elongation occurred at high coiling temperature, Luder's bands clearly existed in 4A1C and 4B1C.

Table 7. Energy absorbed at Charpy test (t = 0c)

	ftxlb	Joules		ftxlb	Joules
2A1C	47	64	2B1C	44.5	60
2A2C	31.5	43	2B2C	29	39
2A3C	30.5	41	2B3C	24	33
2A4C	40	54	2B4C	34	46

	ftxlb	Joules		ftxlb	Joules
3A1C	39	53	3B1C	33.5	45
3A2C	27	37	3B2C	24	33
3A3C	24	33	3B3C	26.5	36
3A4C	40.5	55	3B4C	23	31

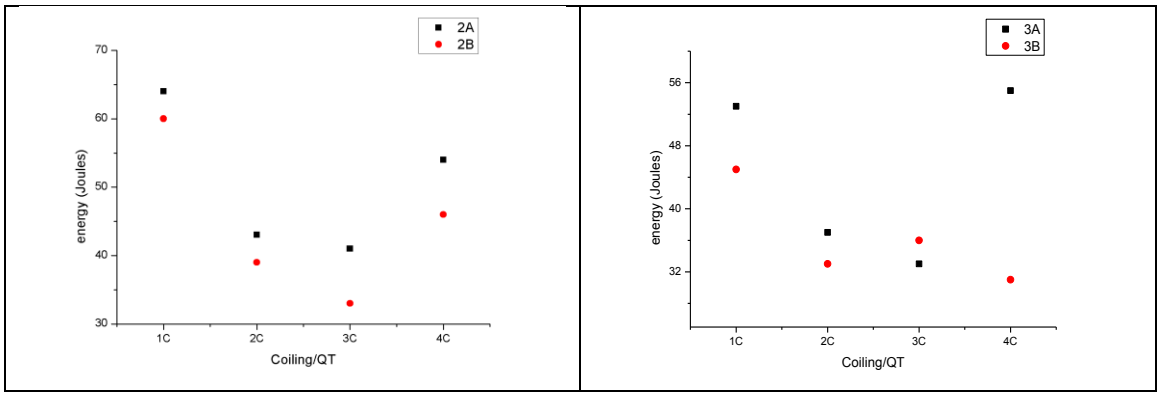

Figure 29. Influence of vanadium addition to the absorbed energy in fracturing

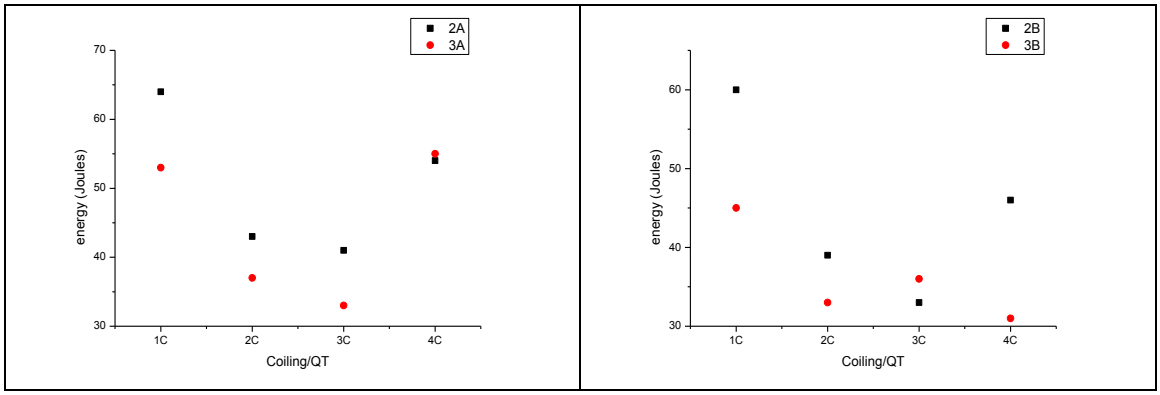

Figure 30. Influence of relative concentration of Al and N to the absorbed energy in fracturing

Table 7 shows the results of the Charpy V-Notch impact test. Figure 29 and 30 show the influence of vanadium addition and relative concentration of Al/N to the energy absorbed during the Charpy test, respectively. In almost all the cases, the addition of vanadium will decrease the energy absorbed in fracturing although V could effectively increase the microhardness and strength.

For high Al/N and low Al/N compositions, the situation is different. In cooling and coiling process, not only the steels with high N and low Al compositions have lower strength but they also absorbed lower energy in fracturing. In quenching and tempering process, variance of absorbed energy between 2A/3A, 2B/3B shows significant different

patterns. It might be due to the different amount of vanadium and would be discussed later.

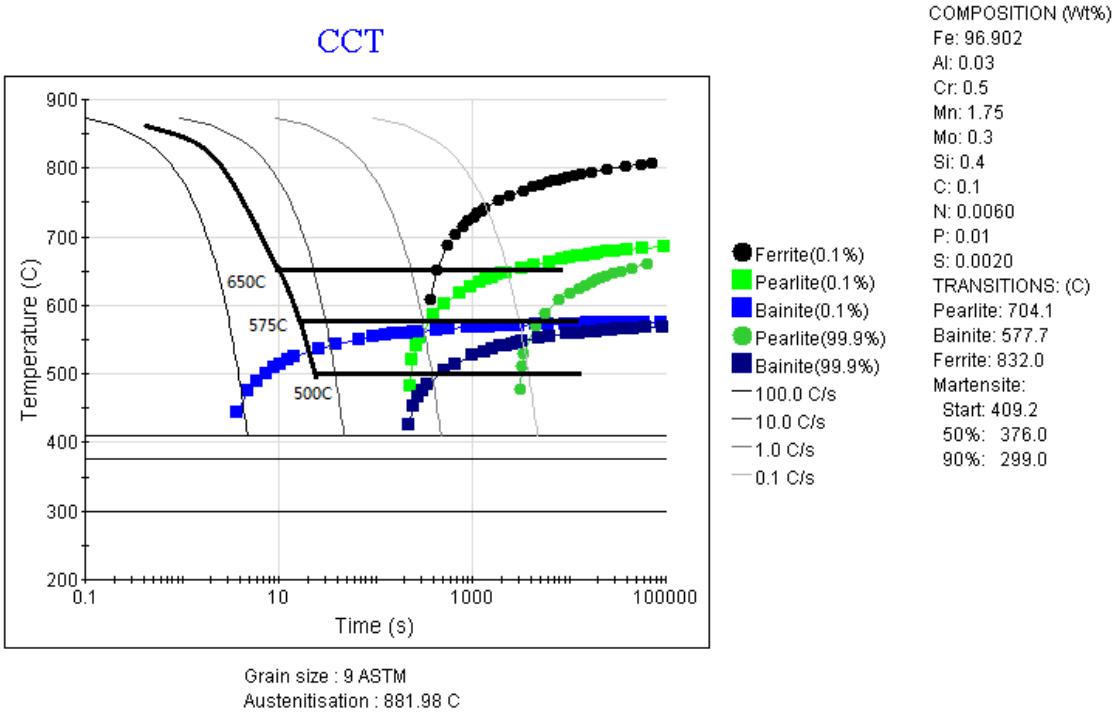

Figure 31. CCT curve of 2A steels which underwent cooling and coiling

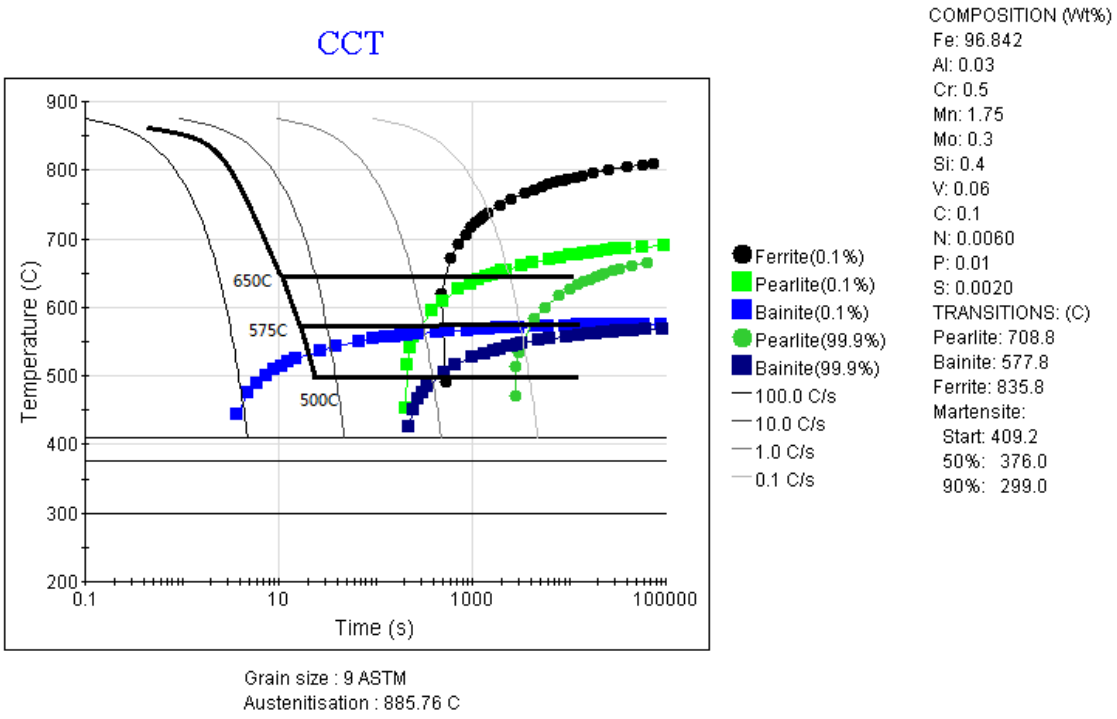

Figure 32. CCT curve of 2B steels which underwent cooling and coiling

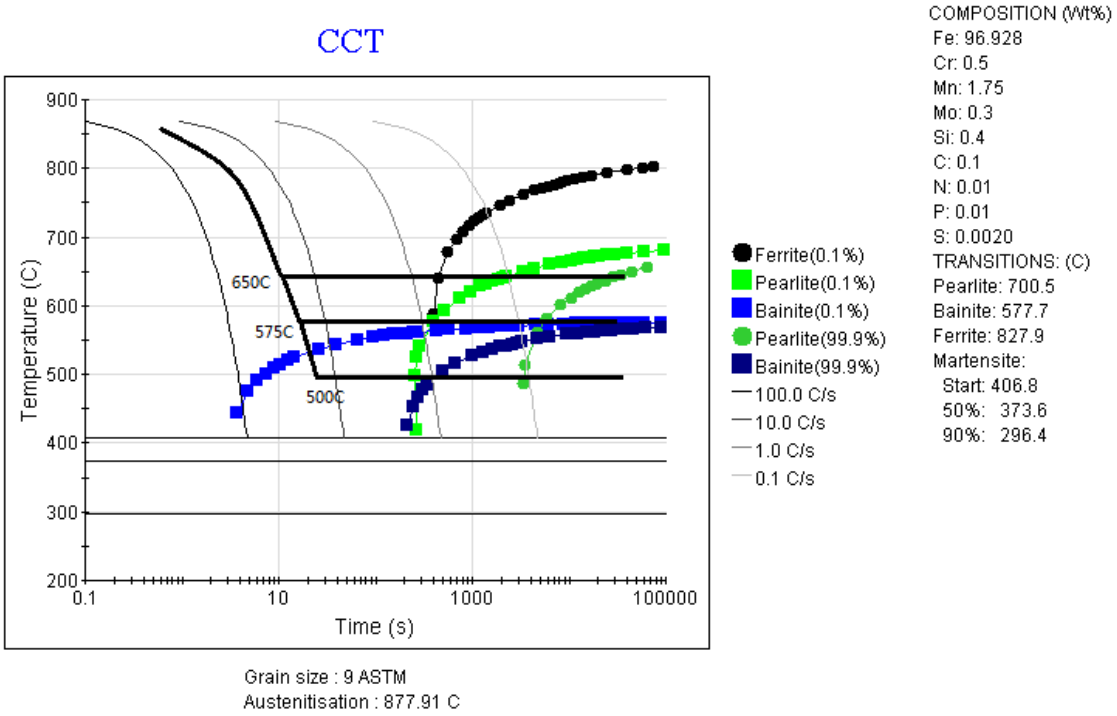

Figure 33. CCT curve of 3A steels which underwent cooling and coiling

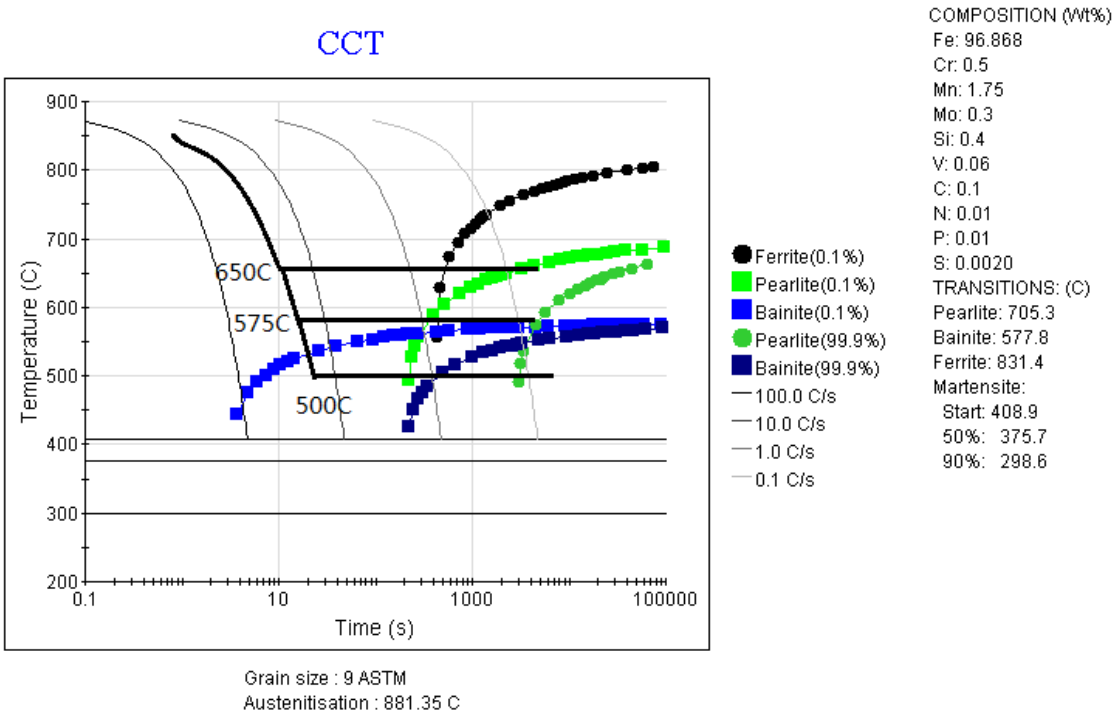

Figure 34. CCT curve of 3B steels which underwent cooling and coiling

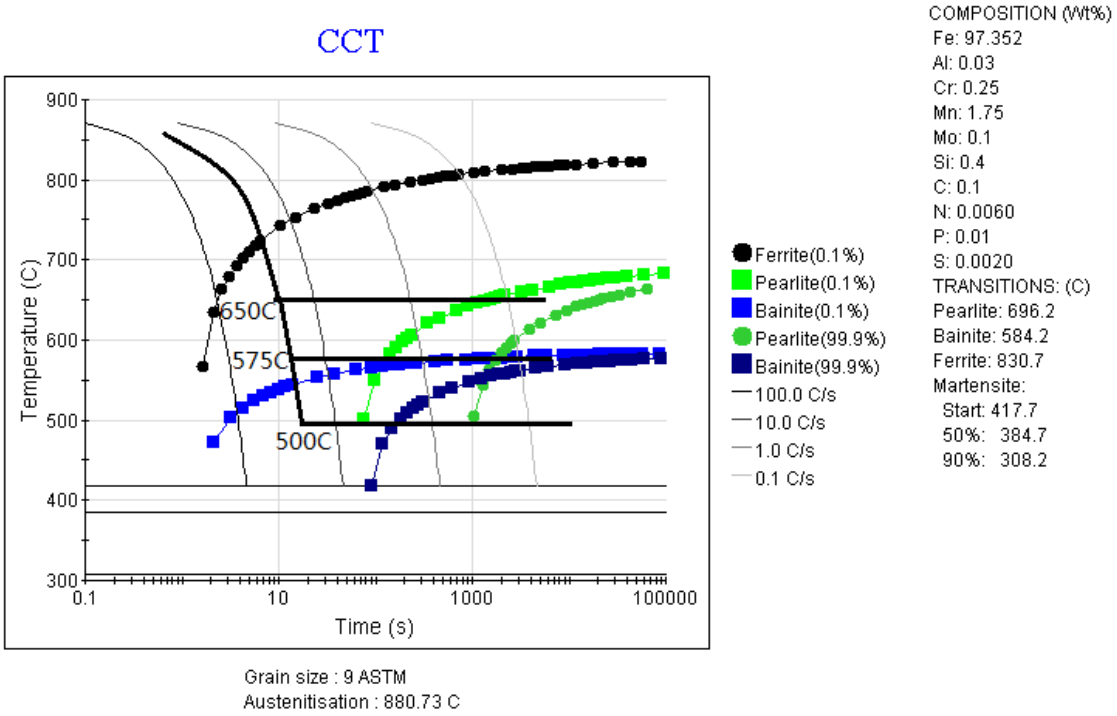

Figure 35. CCT curve of 4A steels which underwent cooling and coiling

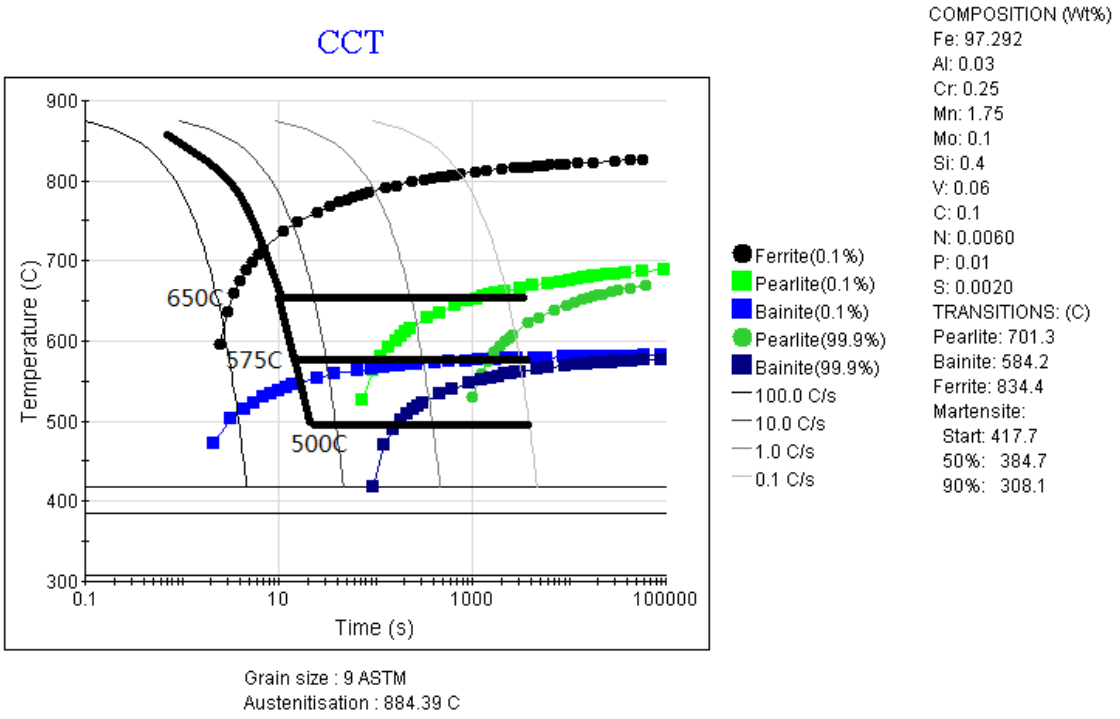

Figure 36. CCT curve of 4B steels which underwent cooling and coiling

Figure 31 – 36 are continuous cooling curves plotted by Jmat-Pro software. The simulated cooling and coiling curves were plotted on each figure. Coiling is regarded as approximation of isothermal transformation, so on the transformation curve, straight line is used to represent the coiling process. From these figures, it can be observed that for series 2 and 3 steels, the major factors that controlled the phase transformation was coiling temperature. At high coiling temperature, cooling and coiling curve intersected with ferrite and pearlite curve. But when coiling temperature dropped, more and more fraction of bainite curves were intersected by the cooling and coiling curve and led to formation of bainitic structure.

The situation was different for the 4 series steels which have the lean alloy composition. The ferrite curves are drastically moved leftward compared with 2 and 3 series, and cooling curves directly intersect with the ferrite curves. This corresponds well with the results obtained from OM and EBSD. Even at the lowest coiling temperature, some polygonal ferrite could still be observed at 4A and 4B. The mechanism will be discussed later.

Apart from chromium and molybdenum, other alloy elements in this study which include Al, V and N do not show great influence on transformation curves. That is the reason for similar morphology observed in 2 and 3 series steels when coiling temperatures were the same.

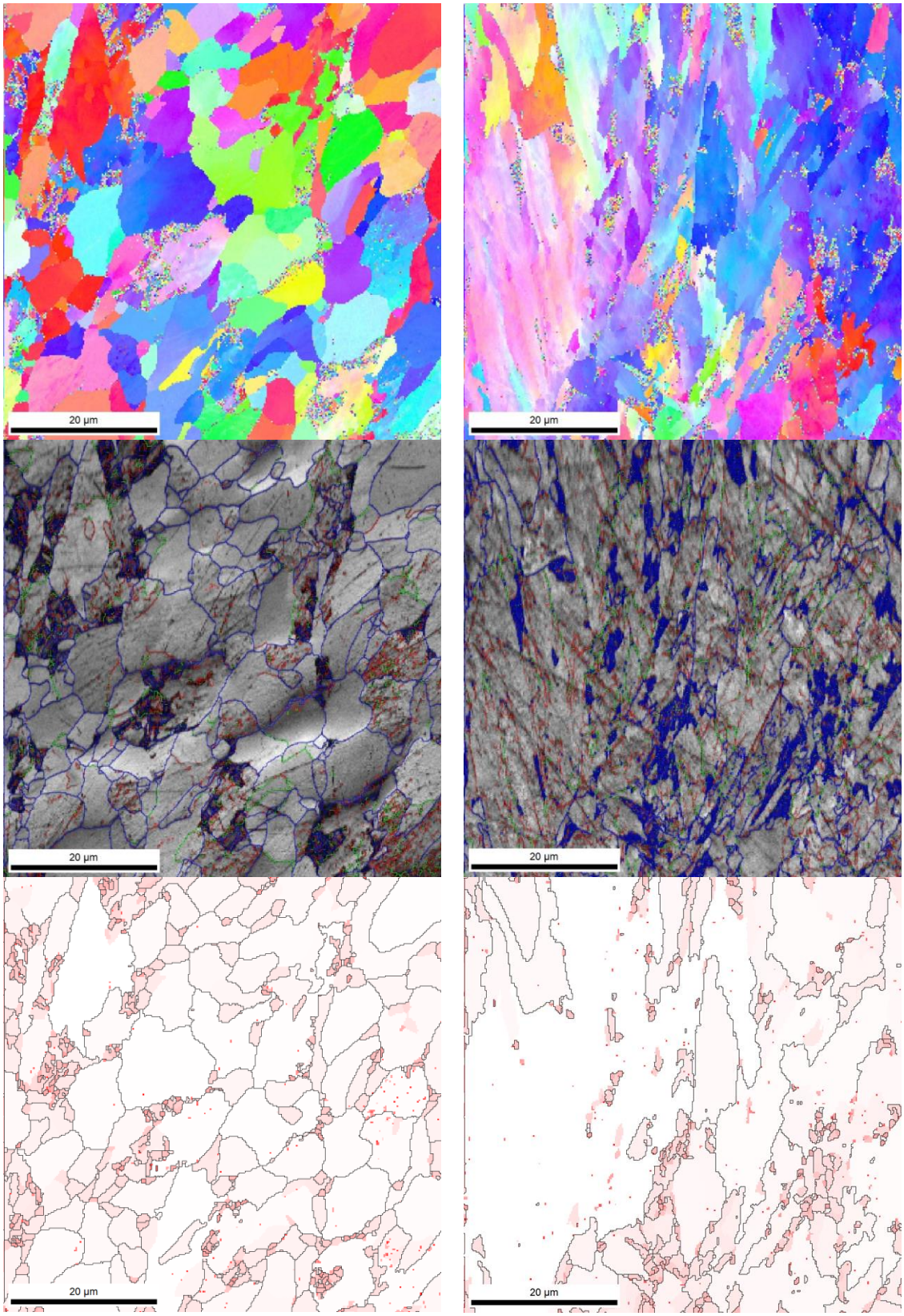

Figure 37. EBSD IPF (up), GB (mid), stored energy (down) map of 2A1C (left), 2A2C (right)

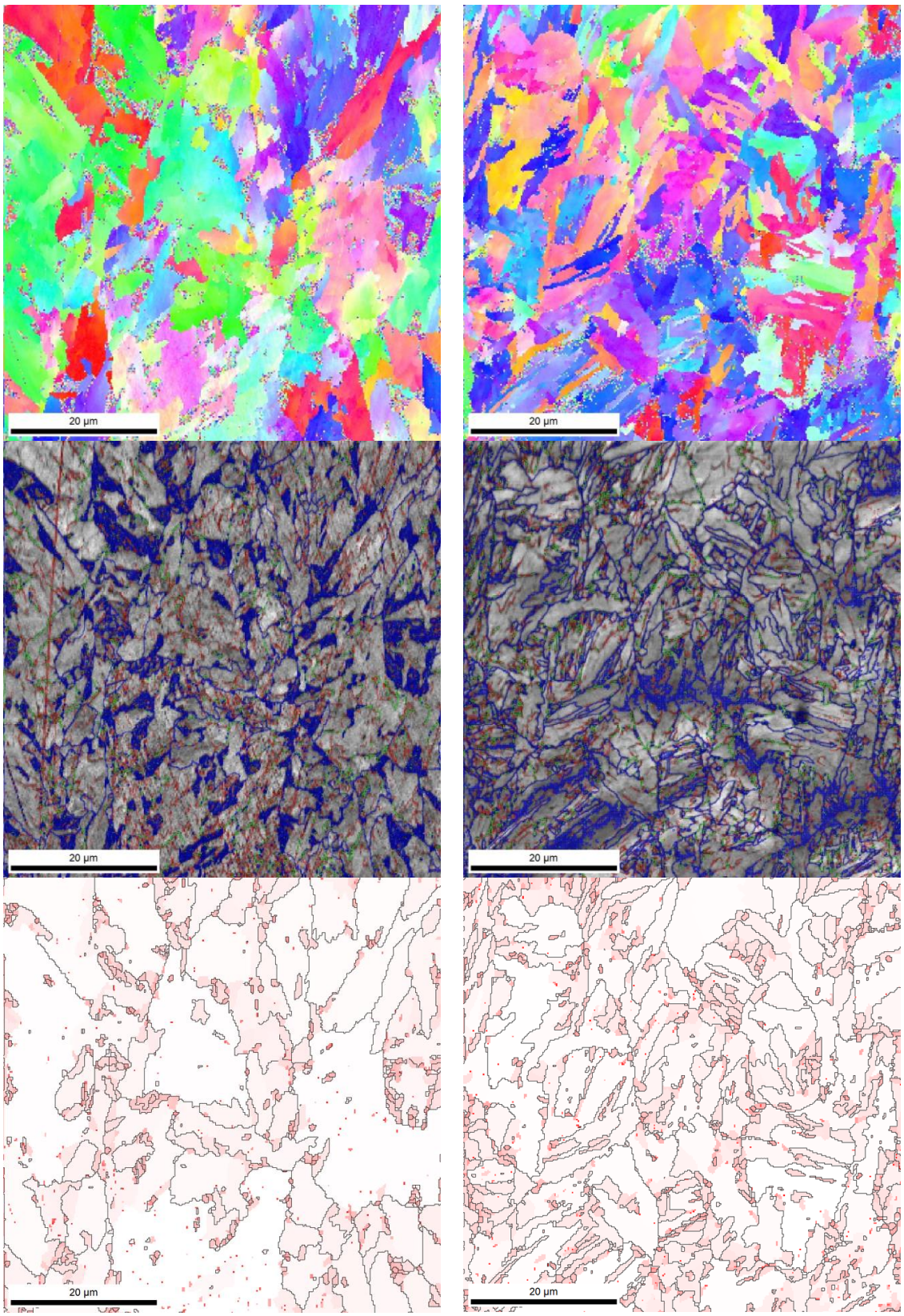

Figure 38. EBSD IPF (up), GB (mid), stored energy (down) map of 3A1C (left), 3A2C (right)

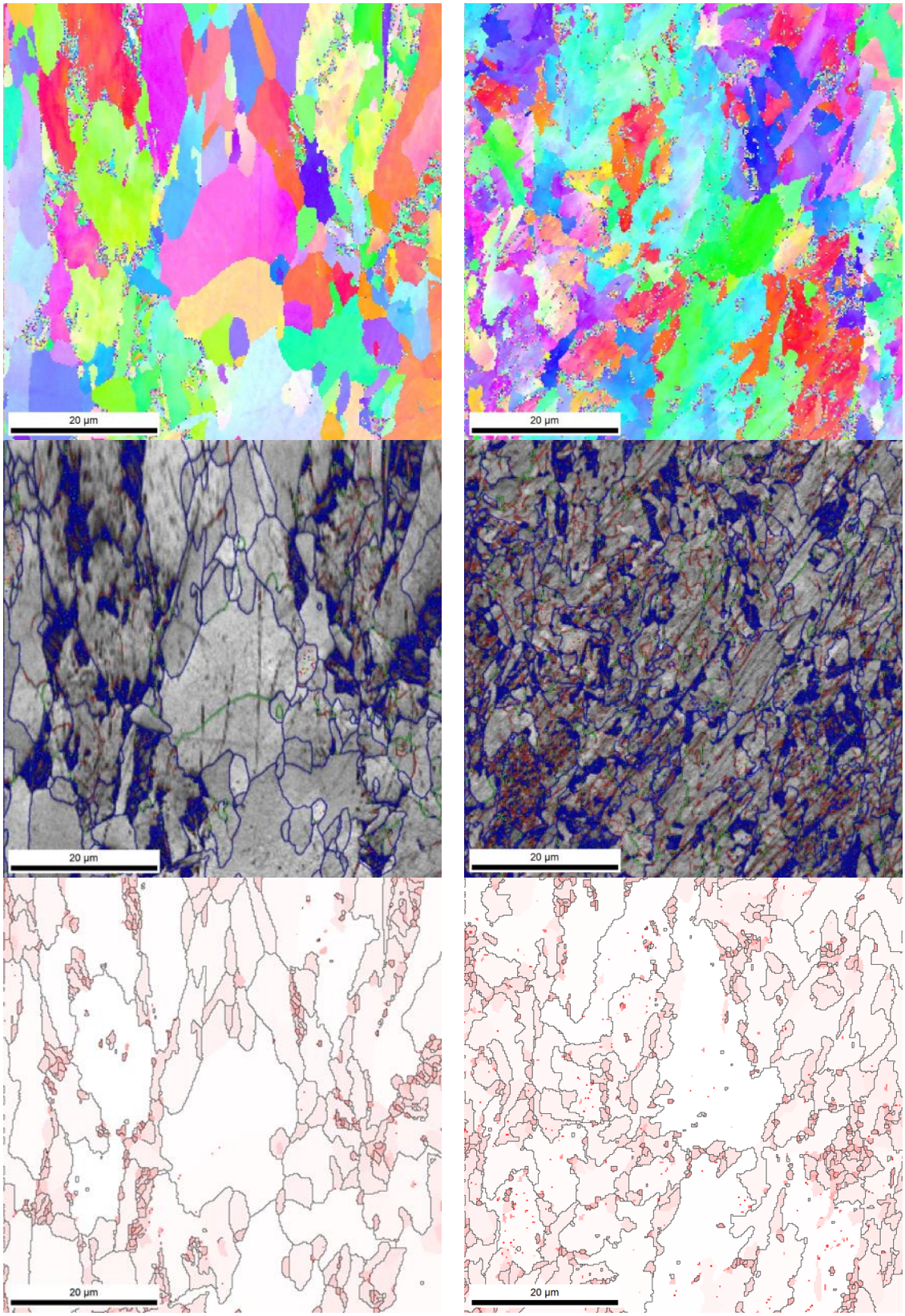

Figure 39. EBSD IPF (up), GB (mid), stored energy (down) map of 2B1C (left), 2B2C (right)

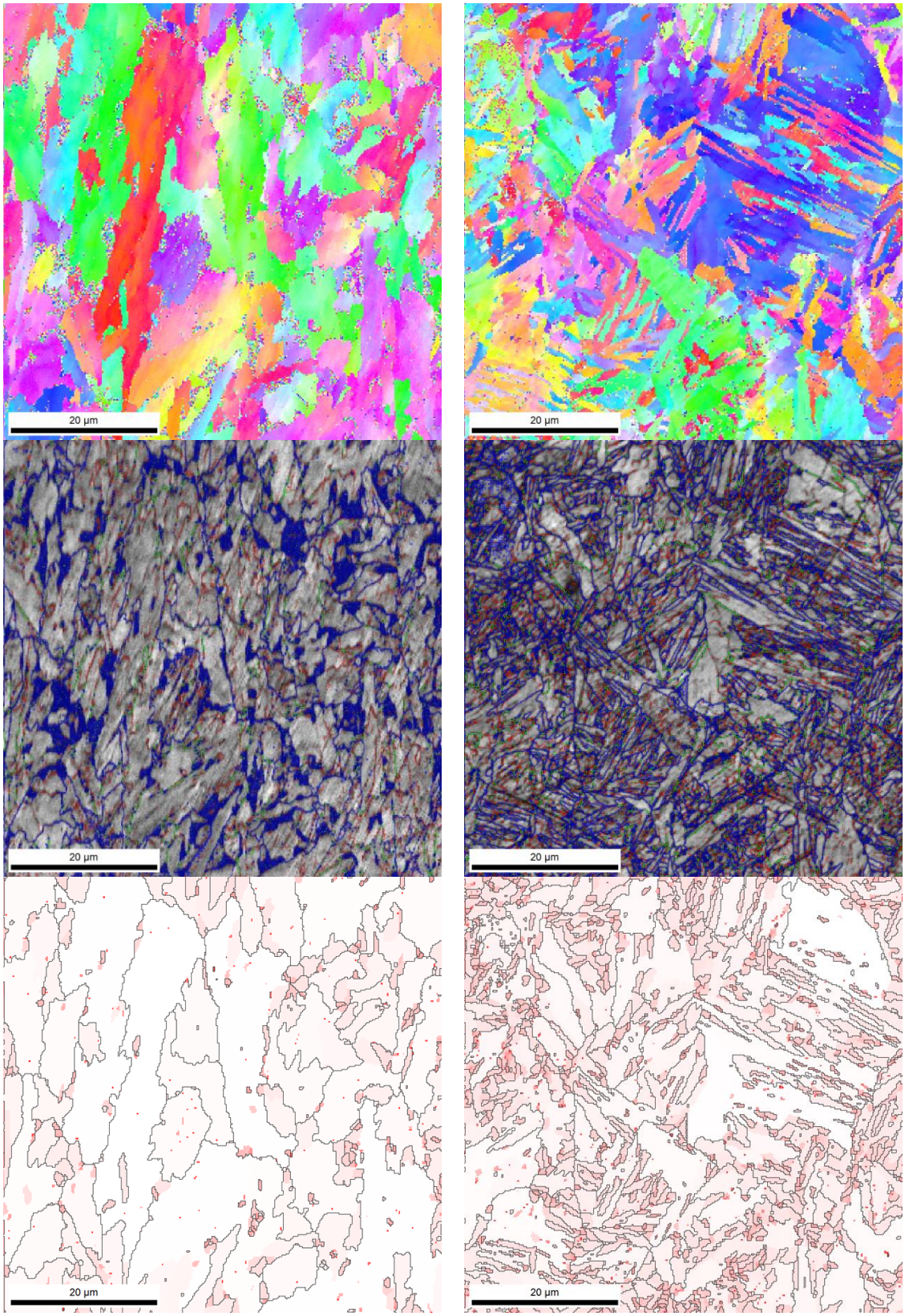

Figure 40. EBSD IPF (up), GB (mid), stored energy (down) map of 2B3C (left), 2B4C (right)

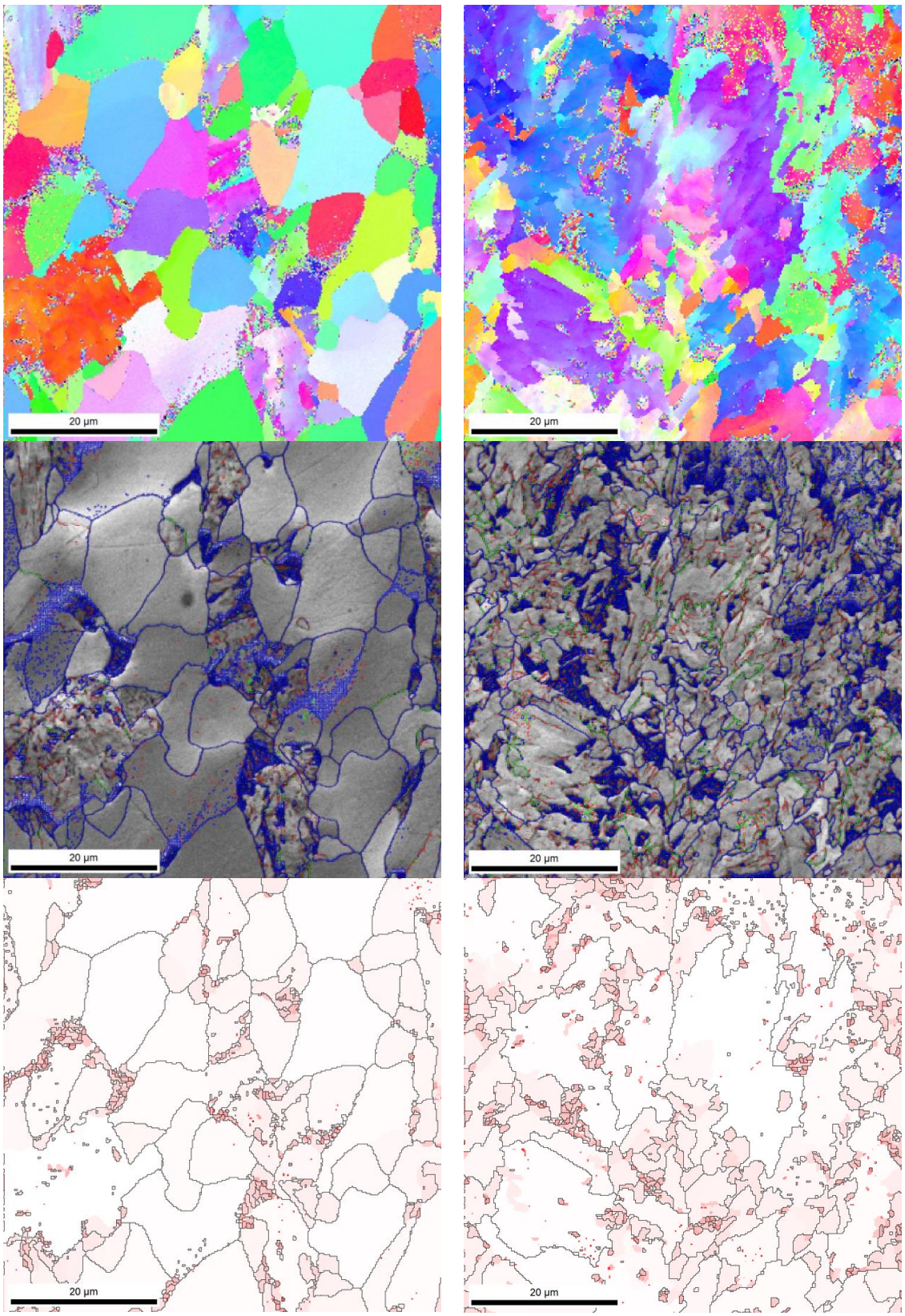

Figure 41. EBSD IPF (up), GB (mid), stored energy (down) map of 3A1C (left), 3A2C (right)

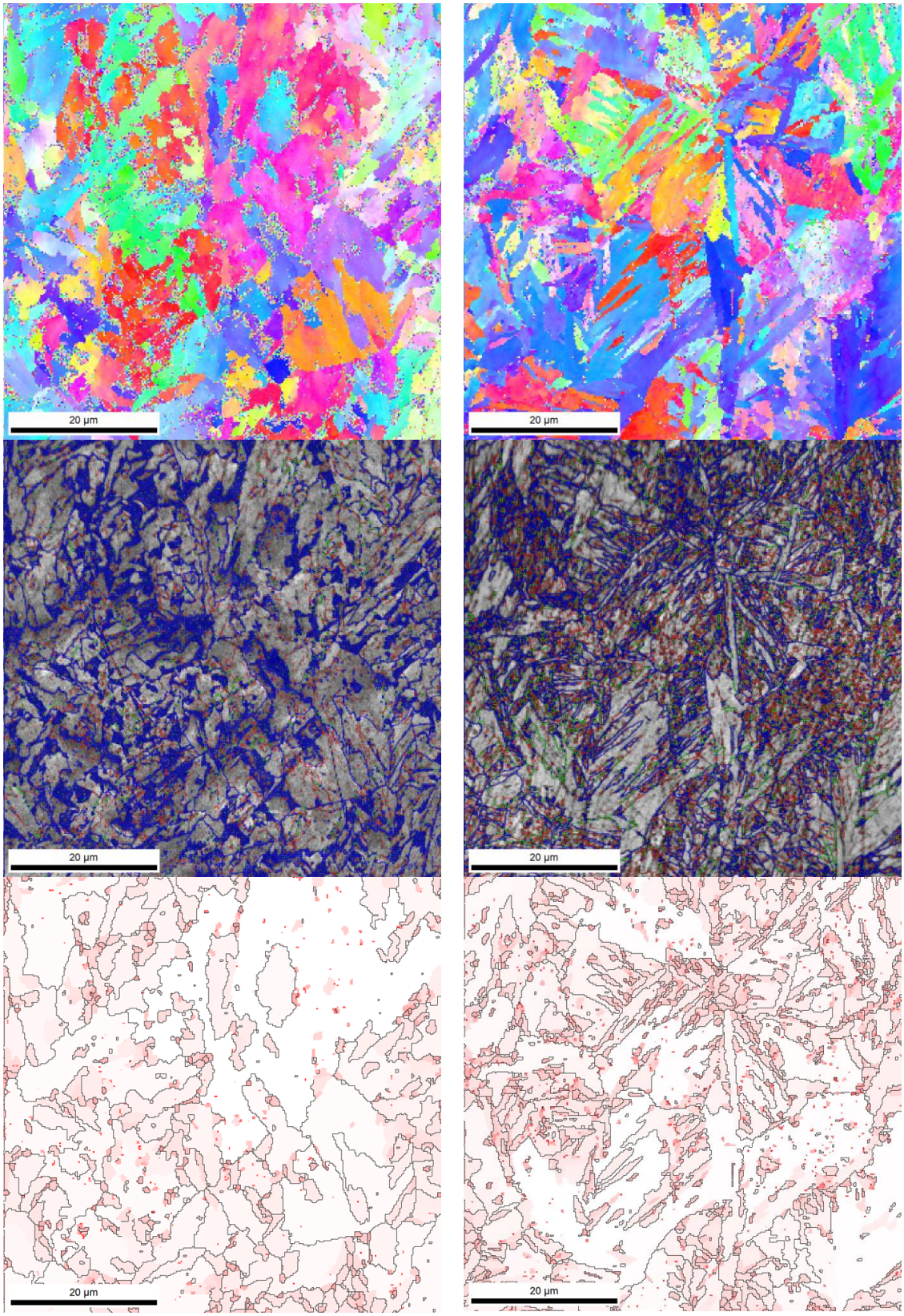

Figure 42. EBSD IPF (up), GB (mid), stored energy (down) map of 3A3C (left), 3A4C (right)

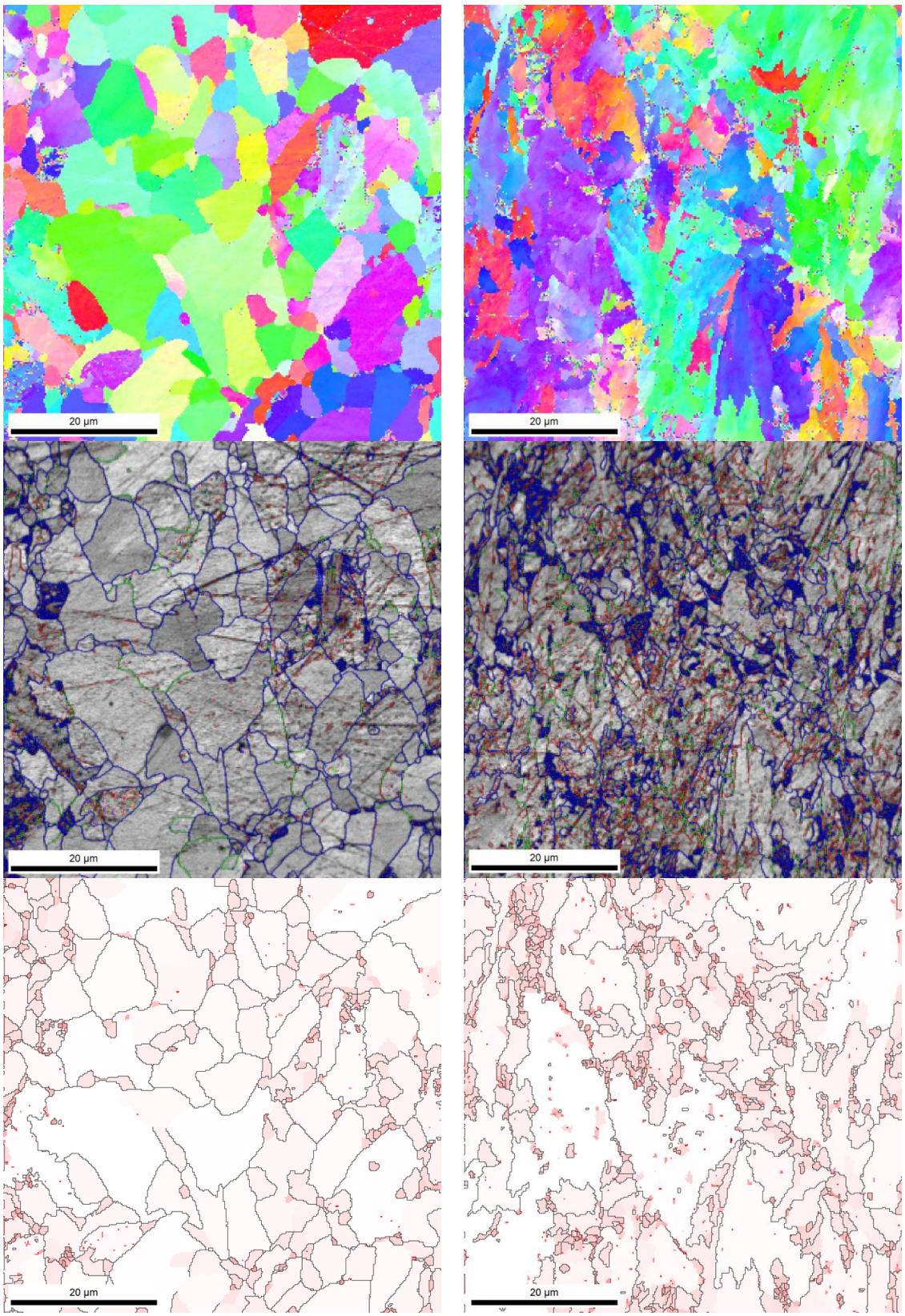

Figure 43. EBSD IPF (up), GB (mid), stored energy (down) map of 3B1C (left), 3B2C (right)

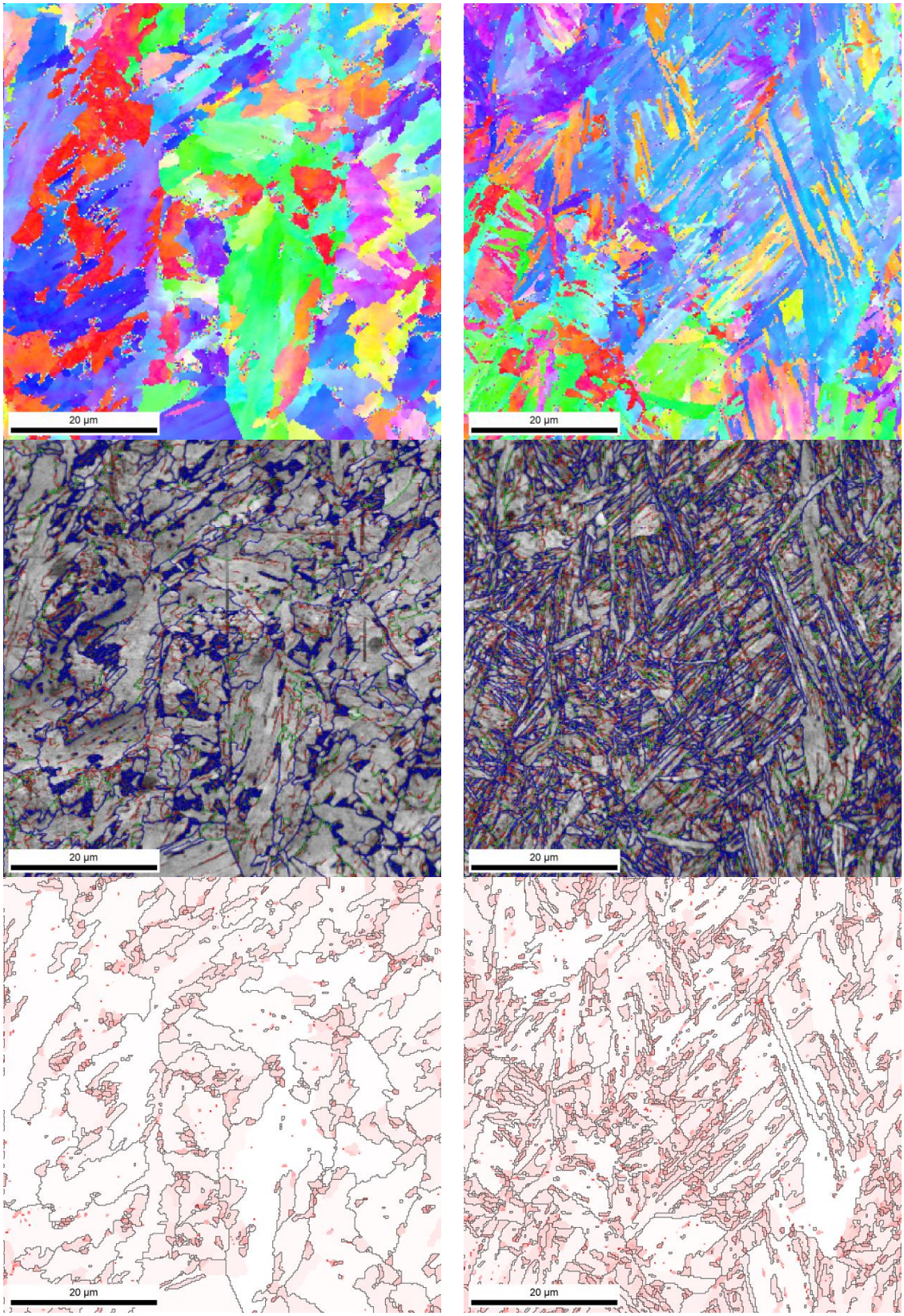

Figure 44. EBSD IPF (up), GB (mid), stored energy (down) map of 3B3C (left), 3B4C (right)

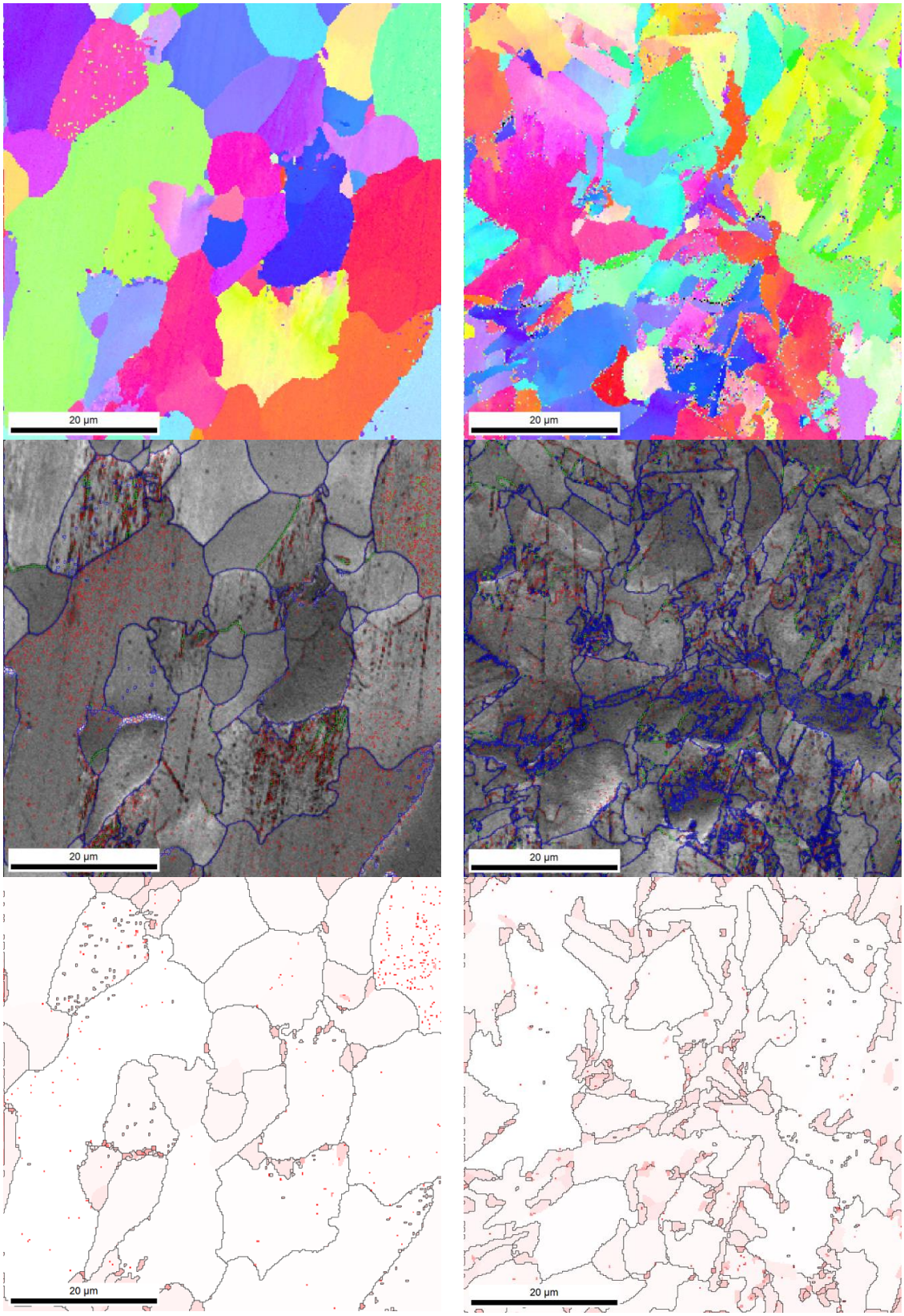

Figure 45. EBSD IPF (up), GB (mid), stored energy (down) map of 4A1C (left), 4A2C (right)

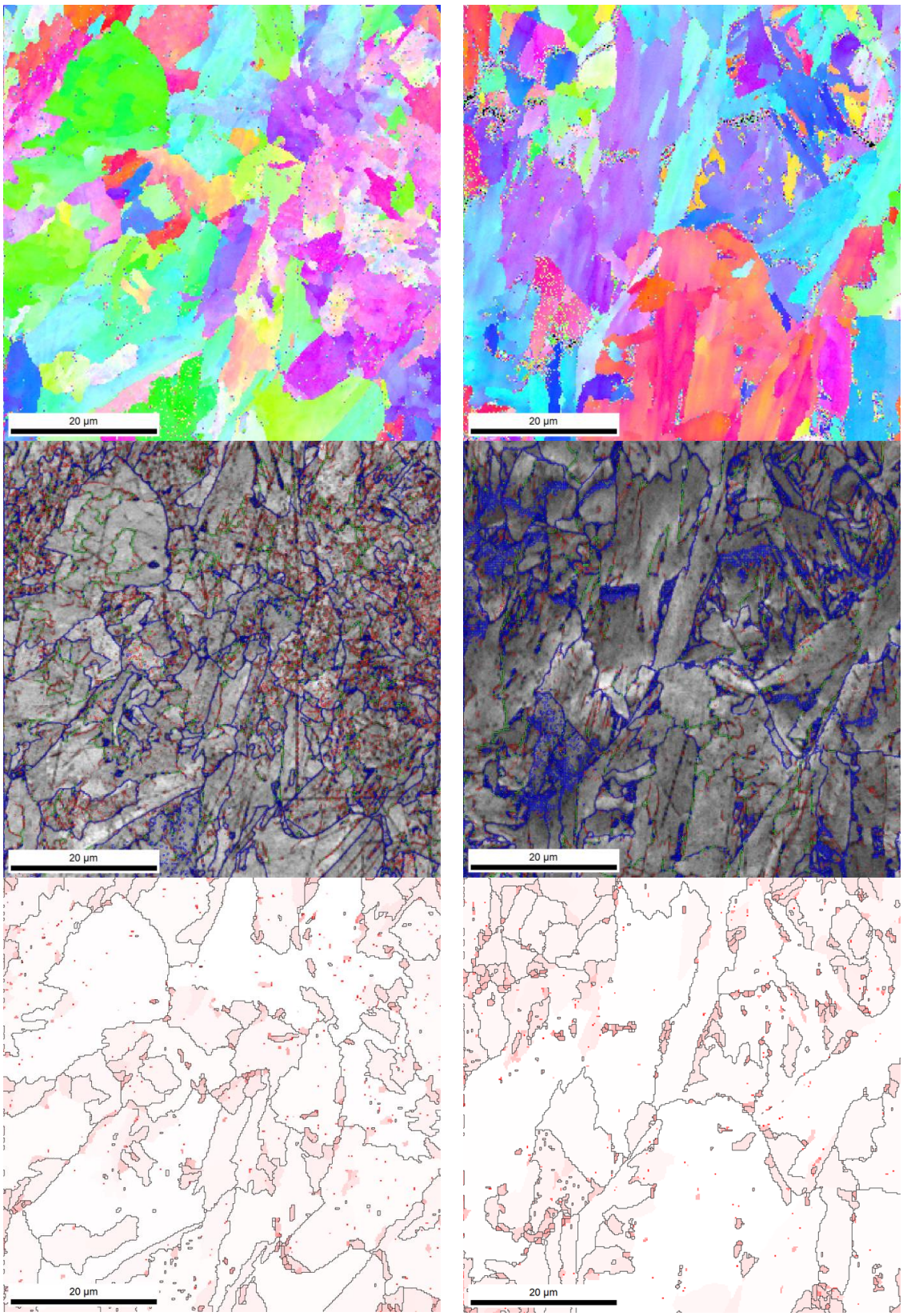

Figure 46. EBSD IPF (up), GB (mid), stored energy (down) map of 4A3C (left), 4A4C (right)

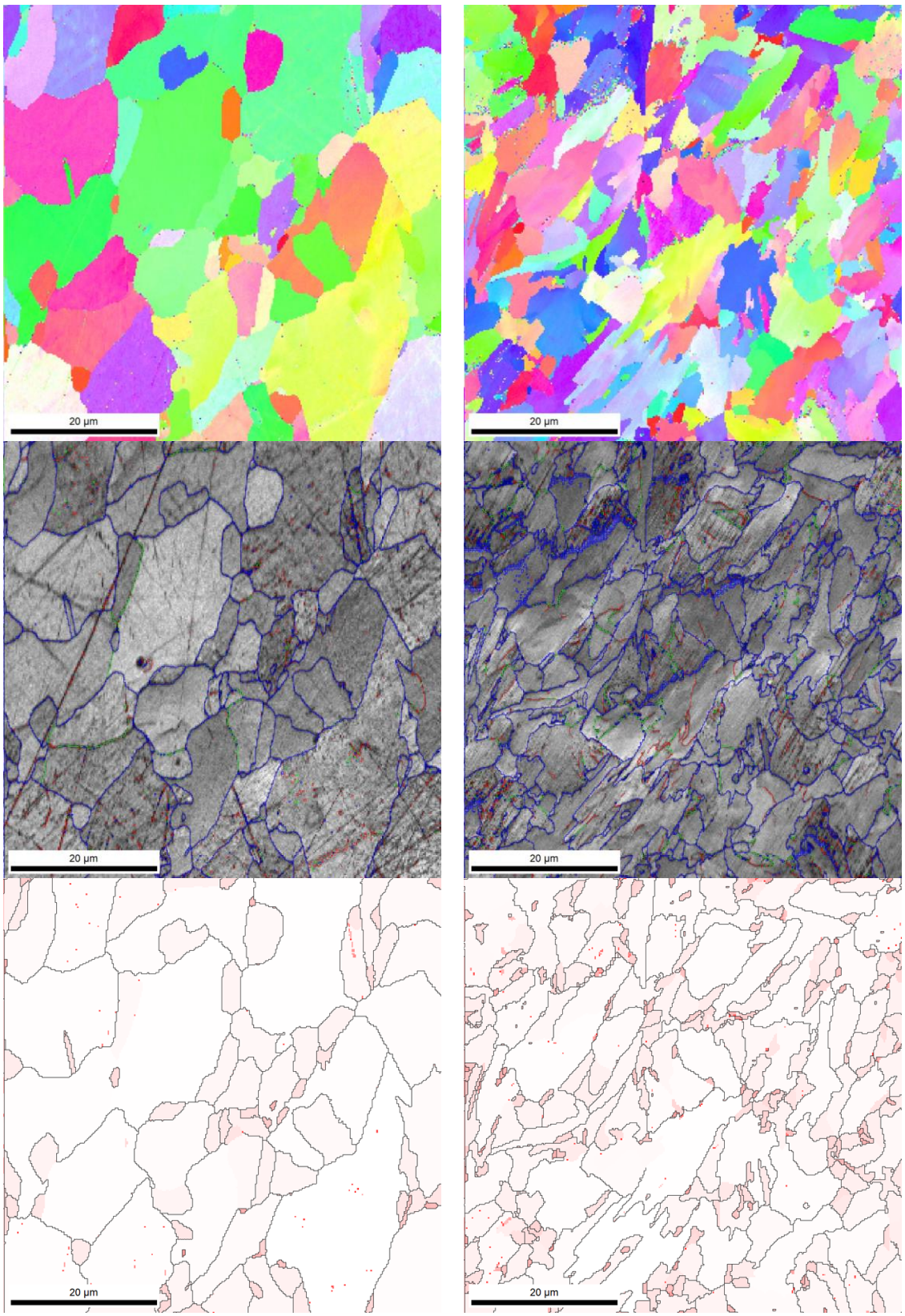

Figure 47. EBSD IPF (up), GB (mid), stored energy (down) map of 4B1C (left), 4B2C (right)

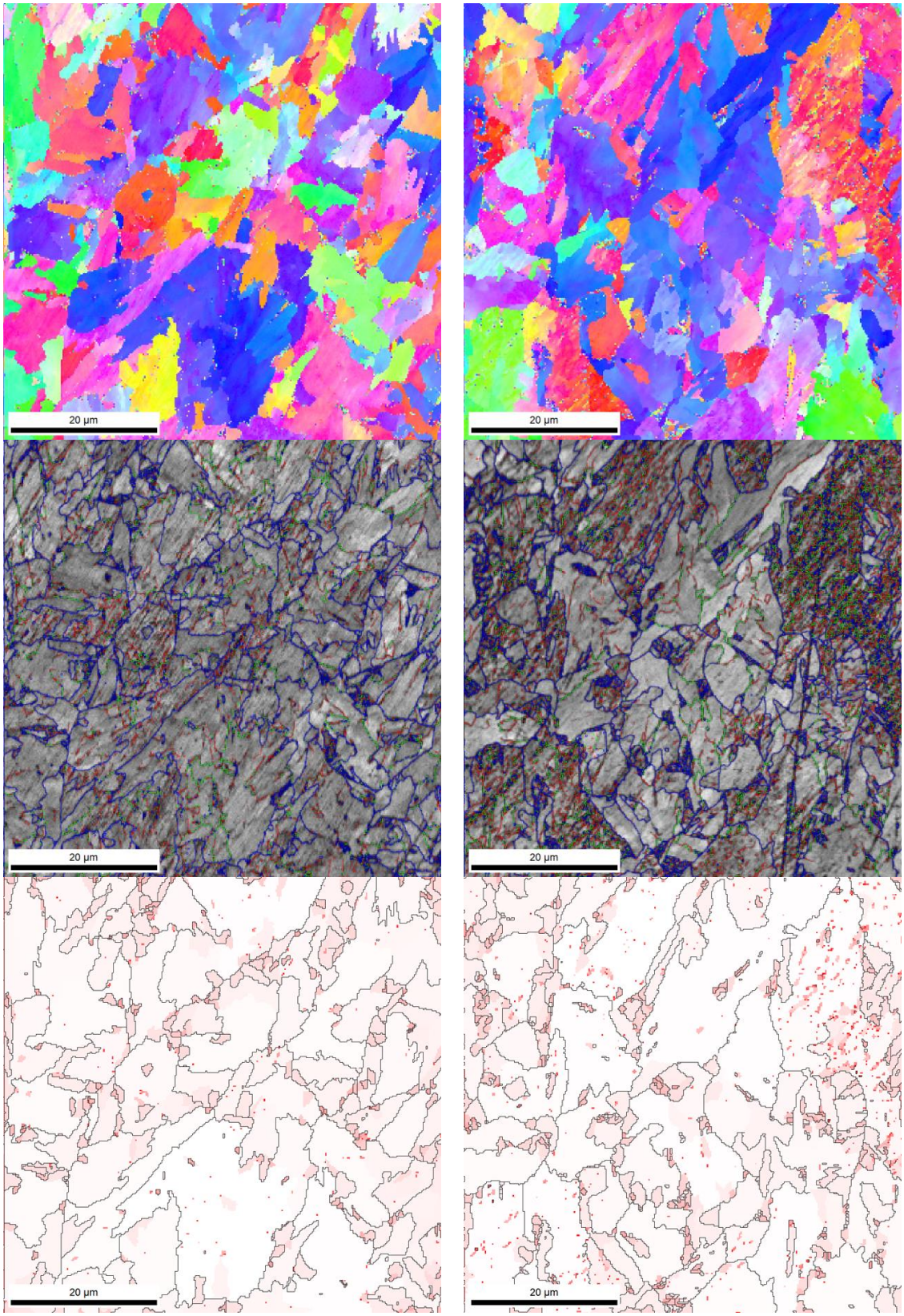

Figure 48. EBSD IPF (up), GB (mid), stored energy (down) map of 4B1C (left), 4B2C (right)

Table 8. Stored energy of steels in different grades

Steel grades	Stored energy/J	Steel grades	Stored energy/J
2A1C	1.04	**2B1C**	0.92
2A2C	0.74	**2B2C**	1.12
2A3C	0.98	**2B3C**	0.77
2A4C	1.44	**2B4C**	1.71
3A1C	0.77	**3B1C**	0. 93
3A2C	1.03	**3B2C**	1. 17
3A3C	1.06	**3B3C**	1. 07
3A4C	1.65	**3B4C**	1. 75
4A1C	0.46	**4B1C**	0. 51
4A2C	0.75	**4B2C**	0. 98
4A3C	0.76	**4B3C**	0. 93
4A4C	0.79	**4B4C**	1. 07

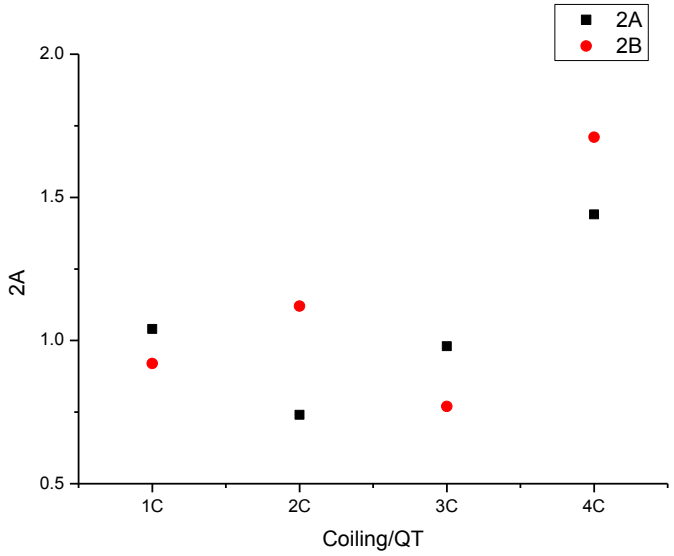

Figure 49. Stored energy comparison of 3A and 3B

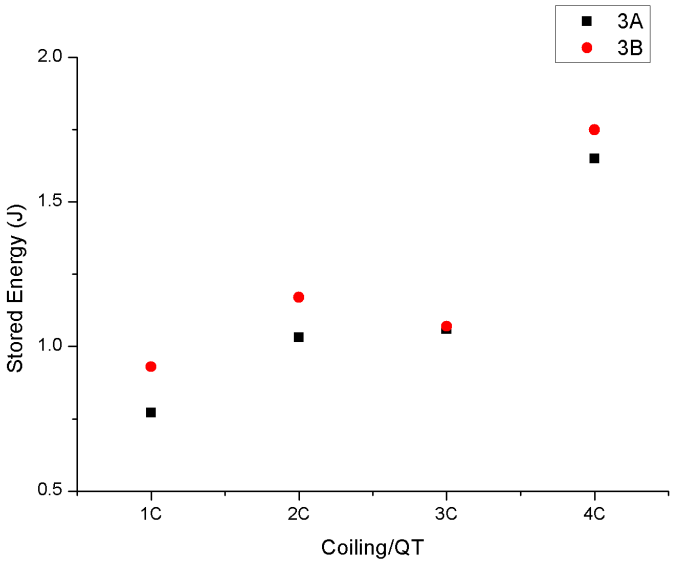

Figure 50. Stored energy comparison of 3A and 3B

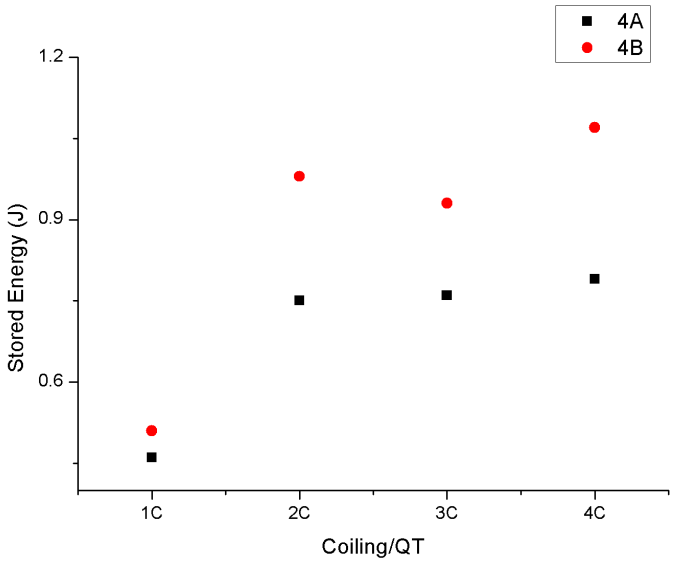

Figure 51. Stored energy comparison of 4A and 4B

The changing trends of stored energy of almost all series steels are similar to each other. At highest coiling temperature (1C), the stored energy was the lowest one. Also, according to the grain boundary map, the grain boundary distribution was also relatively sparse. At the intermediate coiling temperature (2C), the stored energy significantly increased. From inverse pole figures, it can be seen that the morphology of microstructures experienced great changes, from polygonal ferrite to non-polygonal ferrite and some bainitic structures. At the lowest coiling temperature (3C), the stored energy value was near to the intermediate ones, the morphology obtained from inverse pole figures also resembled with the 2C. For the quenching and tempering steels (4C), the stored energy was highest in all cases, and in 2 and 3 series samples, the martensite laths can be clearly observed.

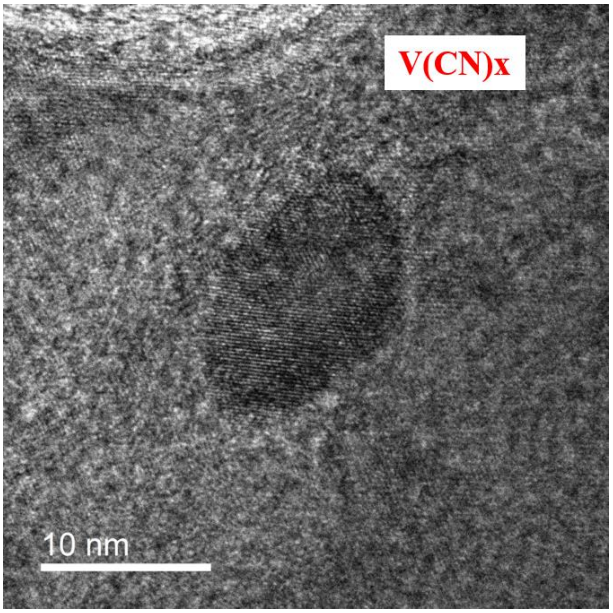

Figure 52. V(CN) precipitate in ferrite of 2B1C, CT=650C

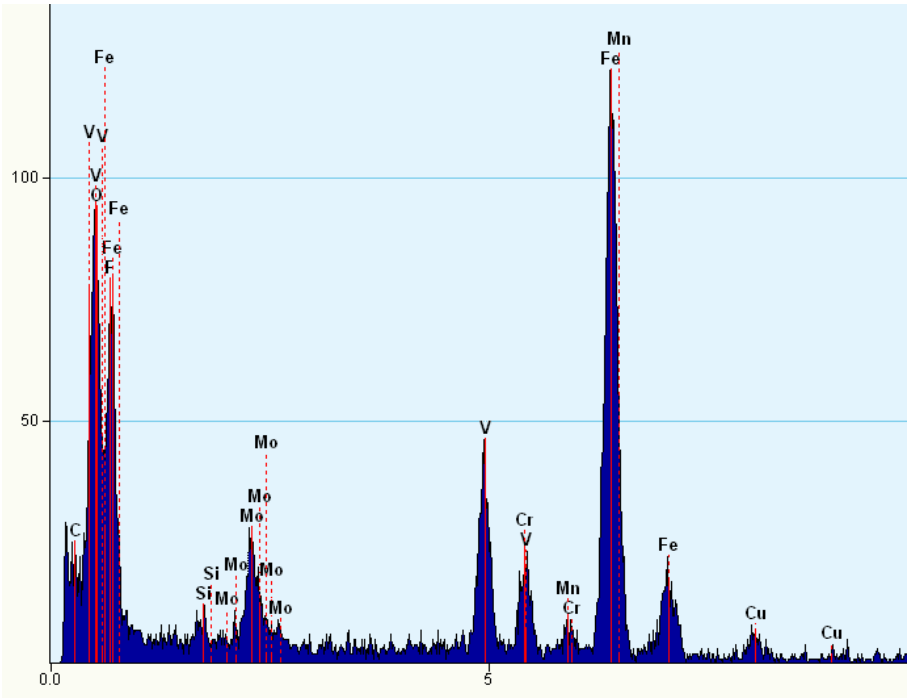

Figure 53. EDAX analysis results of precipitates in ferrite(2B1C)

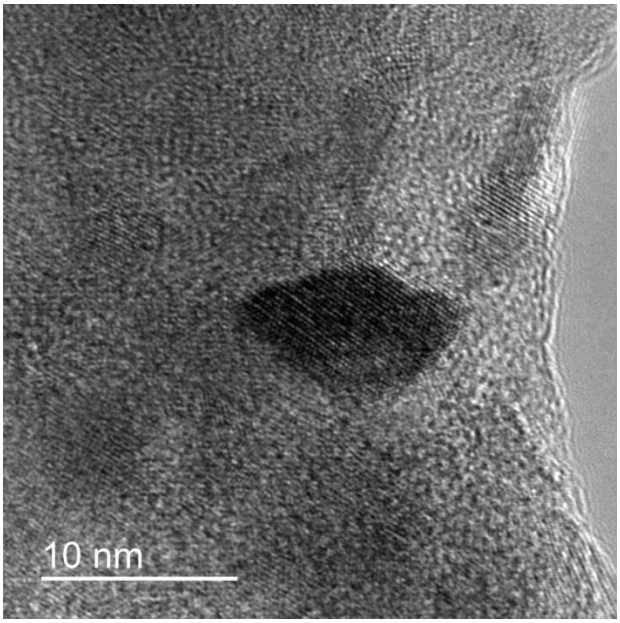

Figure 54. V(CN) precipitate in ferrite of 3B1C, CT=650C

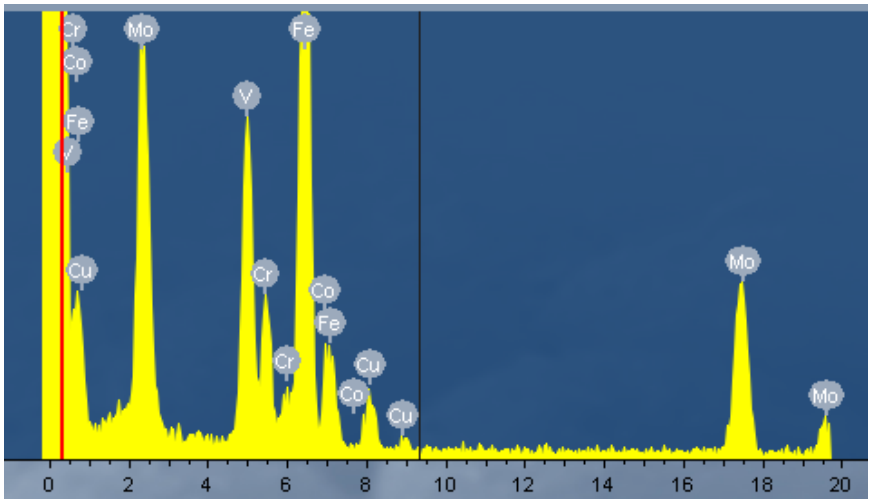

Figure 55. EDAX analysis results of precipitates in ferrite(3B1C)

From the TEM results above, it could be seen that the size of precipitates is about 10nm and can effectively enhance the precipitation hardening. The vanadium peak is very strong, it means that vanadium played very important role in precipitation hardening in this study. The existence of Cr and Mo peaks proved that these two elements were also significant carbide and nitride formers.

6.0 DISCUSSION

Vanadium is often regarded as a desirable microalloying element for precipitation strengthening in recrystallization controlled rolling. Because it provides a relatively small increase of recrystallization stop temperature and it is an effective ferrite strengthening element. Nitrogen is an important element in controlling the precipitation of vanadium carbonitrides due to the much lower solubility product of VN. In thermomechanical processing of hot rolled band, the coiling temperature is an important parameter because it has great influence on microstructures and mechanical properties. The additions of Cr and Mo are also important since they help increase hardenability causing ferrite to form at lower temperatures. This ferrite formed at lower temperatures is very high in dislocation density, higher than polygonal ferrite and much harder as well. The Cr and Mo also appear to contribute to higher precipitation hardening since they are found in the VCN precipitate. This study was designed to investigate the factors listed above, and they will be discussed one by one.

1) Vanadium can effectively improve the strength and hardness of hot rolled steels at high coiling temperature, but the effectiveness decreases with decreasing coiling temperature. The main reason for this variation in strengthening is caused by the changing nature of the ferrite formed with falling coiling temperatures. The ferrite formed at high coiling temperatures

is polygonal ferrite which forms by the reconstructive or diffusion controlled mechanism. The high transformation temperatures are conducive to high mobility of the vanadium. Since the VCN lattice does not match well with the ferrite, defects in the ferrite are needed for nucleation. The advancing γ/α interface or transformation front is one form of such defect, leading to sheets of precipitate or interphase precipitation. Dislocations and subgrain boundary walls are another form of defect that can act as VCN nucleation sites. These sites lead to general precipitation arrays. With falling coiling temperature, less and less polygonal ferrite is formed while more non-polygonal or bainitic ferrite is formed by the displacive transformation mechanism. Since the transformation temperature is low, the vanadium has low mobility and few precipitates can form. The major strengthening found displacively formed low temperature ferrite is dislocation strengthening. Vanadium would be expected to have a minor role in strengthening low temperature ferrite, mainly through solid solution strengthening. Therefore, it is clear that vanadium plays very different roles in strengthening ferrite formed at high or low coiling temperatures, and would be expected to be very important at higher coiling temperatures but not at lower temperatures. This is what, in fact,, has been observed.

2) The images of optical microscopy and inverse pole figures from EBSD show that the vanadium addition did not have great influence on the morphology of microstructures. At the meantime, vanadium did not provide extra benefits for austenite grain refinement. At high coiling temperature, the difference of grain

size of the same series steels was relatively small. The reheating temperature in TMP process largely exceeded the grain coarsening temperature of vanadium, at 1250C the austenite growth of steels with vanadium addition would even exceed the growth of normal C-Mn steels[35]. Under this situation, the vanadium addition would not be able to inhibit the grain coarsening.

3) Although it was believed by many researchers that high nitrogen composition in microalloyed steels with vanadium addition could effectively increase the precipitates density of V (CN) and enhance the precipitation strengthening. In this study, the results showed increase nitrogen and decrease aluminum concentration simultaneously would not increase final strength in hot strip. At highest coiling temperature, strength and hardness of 2 series (high Al, low N) and 3 series (high N, low Al) are almost the same. At the intermediate and low coiling temperature, strength and hardness of 2 series steels even exceeded the 3 series steels and this was beyond the previous expectation. As indicated in Table 5, at high coiling temperature, the grain size of 2 series was much smaller than 3 series, and according to OM images as well as inverse pole figures, 3A1C and 3B1C has a strong tendency for grain coarsening. The reason is the grain coarsening temperature of Al is much higher than V, and even though the solubility product of AlN is lower than VN. In this case, steels with high Al concentration would have larger pinning force to retard the grain coarsening. In this case, at high coiling temperature, enhancing vanadium precipitation hardening has been offset by significant increase of grain size led by reduction of aluminum. At lower coiling temperature, the

effectiveness of interphase precipitation hardening of vanadium became weaker, while the dislocation strengthening would remain high.

4) In all experiments, vanadium showed very good tempering resistance in quenching and tempering steels. The microhardness and strength of QT steels with vanadium addition is much higher than those without vanadium addition. Vanadium effectively enhance the secondary hardening. Finely dispersed vanadium carbides precipitated out in tempering retarding the motion of dislocation and reducing the softening and the growth rate of ferrite grains and hence increase the final strength.
5) Cr and Mo are important alloy elements in steels. They participate in the strengthening of materials with various mechanisms which include increasing hardenability (leading to more and harder low temperature ferrite), and precipitation hardening. Also, Cr and Mo are very effective in tempering resistance. In this study, the results show that strength and microhardess of the steels with lower concentration of Cr and Mo were dramatically lower than the higher ones. At the meantime, due to the lack of carbide and nitride formers, the nitrogen and carbon atoms segregate into dislocations and impede their movements. So, at high coiling temperature, steels with lean composition underwent yield point elongation, and Luder's bands could be observed.
6) Different processing conditions led to significant difference in microstructures and mechanical properties. In this study, for cooling and coiling processes, lowering the coiling temperature would change the major microconstituent from polygonal ferrite and pearlite to non – polygonal ferrite and bainite, and

with an increase in the strength and hardness. The continuous cooling transformation curve plotted by JmatPro verified this changing trend. The microstructures formed in low coiling temperature had higher density of dislocations and grain boundaries, and this was confirmed by the stored energy distribution maps and grain boundary distribution maps. The stored energy reflected the density of defects which played very important roles in increasing strength. In this study, the stored energy distribution in different grades of steels generally corresponds to the change of strength and hardness but a few exceptions also existed. The reason might be the problem of stored energy calculation algorithm of the software. For example, the pearlite structure was regarded as aggregation of high angle grain boundary (This also could be seen in grain boundary distribution map), so the stored energy corresponded to pearlite region was very high although actually it was not the case. For quenching and tempering steels, the major microconstituent was tempered martensite, and the lath structures as well as prior austenite grain boundary could clear be seen in IPF map, and the stored energy was also the highest ones.

7) In cooling and coiling process, the addition of vanadium would impair the impact toughness at a given temperature. Also, high N low Al composition would have detrimental effects on the fracture toughness in this study. This may due to the enhanced V(C, N) precipitation hardening led by addition of vanadium or nitrogen. Another important factor that may influence the toughness is grain size. The grain size of steels with high N low Al

composition is much coarser than the high Al and low N ones as discussed before. This will also result in reduction of absorbed energy in the Charpy test. In the quenching and tempering process, it can be seen that the variance of absorbed energy between 2A and 3A is much smaller than that of 2B and 3B. The reason might be different amount of vanadium in different group. For 2B and 3B, higher concentration of vanadium will lead to more formation of V-carbonitrides precipitates which will cause the loss of toughness. As discussed before, nitrogen concentration directly determines density of vanadium based precipitates, so high N composition would definitely yield more V(C, N) precipitates and absorb much lower energy in fracturing. On the other hand, low V concentration would have much less V-based precipitates, so the difference of toughness between 2A and 3A would also be much less.

7.0 CONCLUSION

This study investigated several factors which include processing conditions and chemical compositions that may influence the properties and microstructures of hot rolled microalloyed steels. Based on experiment results and analysis, the following conclusion could be made:

1) Vanadium is a very effective ferrite strengthening element. A small amount addition of vanadium could significantly improve the strength and microhardness of steels with ferrite-pearlite structure.
2) When distribution of ferrite decreased and bainitic structures increased, the effectiveness of vanadium would also decrease because the vanadium carbonitrides that could be used for precipitation strengthening generated at the boundary of austenite and ferrite, either for general precipitation or interphase precipitation.
3) In this study, increasing concentration of nitrogen and decreasing concentration of aluminum would not help to improve the final strength. Although the precipitates density of vanadium carbonitrides might be increased by increasing nitrogen contents, but it would sacrifice the grain refinement effects led by aluminum addition. Even in high vanadium

concentration composition, the vanadium contents were still relatively low and this might also contribute to this result.

4) Vanadium played very important role in tempering resistance. Vanadium carbides precipitated out in the process of tempering effectively enhance the secondary hardening and improve the strength and hardness of QT steel.
5) Lowering the concentration of Cr and Mo would result in dramatic decrease in strength. Also, yield point elongation would occur in steels with low alloy concentration because of the lack of carbide and nitride formers and increasing amount of interstitial elements.
6) Changing coiling temperature would significantly change the microstructures of hot band. Lowering coiling temperature would lead to more bainitic structures substitute polygonal ferrite and less fraction of ferrite and increase of dislocation and grain boundary density.
7) Although the calculation method and accuracy needs to be improved, stored energy distribution map is still a good way to analyze defects distribution

BIBLIOGRAPHY

1. DeArdo AJ. Modern thermomechanical processing of microalloyed steel: A physical metallurgy perspective. In: *Proceedings of the International Conference "Microalloying*. Vol 95. ; 1995:15-33.

2. Facco G. Effect of cooling rate and coiling temperature on the final microstructure of HSLA steels after HSM and/or laboratory TMP processing. 2009. http://d-scholarship.pitt.edu/7956/.

3. Panigrahi BK. Processing of low carbon steel plate and hot strip - an overview. *Bull Mater Sci*. 2001;24(4):361-371. doi:10.1007/BF02708632.

4. Wilson FG, Gladman T. Aluminium nitride in steel. *Int Mater Rev*. 1988;33(1):221-286. http://www.maneyonline.com/doi/abs/10.1179/imr.1988.33.1.221.

5. DeArdo AJ, Hua MJ, Cho KG, Garcia CI. On strength of microalloyed steels: an interpretive review. *Mater Sci Technol*. 2009;25(9):1074-1082. doi:10.1179/174328409X455233.

6. Zajac S, Siwecki T, Hutchinson B, Attlegård M. Recrystallization controlled rolling and accelerated cooling for high strength and toughness in V-Ti-N steels. *Metall Trans A*. 1991;22(11):2681-2694. doi:10.1007/BF02851362.

7. Riva R, Mapelli C, Venturini R. Effect of Coiling Temperature on Formability and Mechanical Properties of Mild Low Carbon and HSLA Steels Processed by Thin Slab Casting and Direct Rolling. *ISIJ Int*. 2007;47(8):1204-1213. doi:10.2355/isijinternational.47.1204.

8. Park D-B, Huh M-Y, Shim J-H, Suh J-Y, Lee K-H, Jung W-S. Strengthening mechanism of hot rolled Ti and Nb microalloyed HSLA steels containing Mo and W with various coiling temperature. *Mater Sci Eng A*. 2013;560:528-534. doi:10.1016/j.msea.2012.09.098.

9. Baker TN. Processes, microstructure and properties of vanadium microalloyed steels. *Mater Sci Technol*. 2009;25(9):1083-1107. doi:10.1179/174328409X453253.

10. Lagneborg R, Siwecki T, Zajac S, Hutchinson B. The Role of Vanadium in Microalloyed Steels. *Scand J Metall*. 1999;28(5):186-241.

11. Cuddy LJ. The effect of microalloy concentration on the recrystallization of austenite during hot deformation. *Metall Soc*. 1982:129-140.

12. Krauss G. *Steels: Processing, Structure, and Performance*. Asm International; 2005.

13. Benzerga AA, Bre Y. The stored energy of cold work : Predictions from discrete dislocation plasticity. 2005;53:4765-4779. doi:10.1016/j.actamat.2005.07.011.

14. Fang C. Annealing and Precipitation Behavior During Batch Annealing of HSLA Steels. 2011.

15. Titchener AL, Bever MB. The stored energy of cold work. *Prog Met Phys*. 1958;7:247-338.

16. Bohnenkamp K, Lucke K, Masing G. MESSUNG DER LATENTEN VERFORMUNGSENERGIE AN GEZOGENEN KUPFERDRAHTEN. *ZEITSCHRIFT FUR Met*. 1955;46(10):765-770.

17. Clarebrough LM, Hargreaves ME, West GW. The release of energy during annealing of deformed metals. In: *Proceedings of the Royal Society of London A: Mathematical, Physical and Engineering Sciences*. Vol 232. The Royal Society; 1955:252-270.

18. Choi S-H, Jin Y-S. Evaluation of stored energy in cold-rolled steels from EBSD data. *Mater Sci Eng A*. 2004;371(1-2):149-159. doi:10.1016/j.msea.2003.11.034.

19. Wilkinson AJ, Dingley DJ. Quantitative deformation studies using electron back scatter patterns. *Acta Metall Mater*. 1991;39(12):3047-3055. doi:10.1016/0956-7151(91)90037-2.

20. Wu J. Development of a new technique to identify and quantify complex austenite decomposition products. 2005.

21. Humphreys FJ. Review grain and subgrain characterisation by electron backscatter diffraction. *J Mater Sci*. 2001;36(16):3833-3854.

22. Read WT, Shockley W. Dislocation models of crystal grain boundaries. *Phys Rev*. 1950;78(3):275.

23. Hall EO. The deformation and ageing of mild steel: III discussion of results. *Proc Phys Soc Sect B*. 1951;64(9):747.

24. Hansen N. Hall-petch relation and boundary strengthening. *Scr Mater*. 2004;51(8 SPEC. ISS.):801-806. doi:10.1016/j.scriptamat.2004.06.002.

25. Armstrong RW, Codd I, Douthwaite RM, Petch NJ. The plastic deformation of polycrystalline aggregates. *Philos Mag*. 1962;7(73):45-58.

26. Nie J-F. *Physical Metallurgy*.; 2014. doi:10.1016/B978-0-444-53770-6.00020-4.

27. Leslie WC. The physical metallurgy of steels. *Hemisph Publ Corp, 1981,*. 1981:396.

28. Pickering FB. High-strength, low-alloy steels—a decade of progress, Microalloying 75. *Proceedings, Union Carbide Corp, New York*. 1975:9.

29. Gladman T. *The Physical Metallurgy of Microalloyed Steels*. Vol 615. Maney Pub; 1997.

30. Gladman T. Precipitation hardening in metals. *Mater Sci Technol*. 1999;15(1):30-36. doi:10.1179/026708399773002782.

31. Orowan E. Symp. on Internal Stress in Metals and Alloys. *Inst Met London*. 1948:451.

32. Ashby MF. Oxide dispersion strengthening. *Gordon Breach, New York*. 1958:143-147.

33. Astm. Standard Test Methods for Notched Bar Impact Testing of Metallic Materials. 2007;14(C):28. doi:10.1520/E0023-07AE01.2.

34. Dieter GE. Mechanical metallurgy. 2015.

35. Cuddy LJ, Raley JC. Austenite grain coarsening in microalloyed steels. *Metall Trans A*. 1983;14(10):1989-1995.